DEVELOPMENT OF A MODEL AND LOCALIZATION ALGORITHM FOR RECEIVED SIGNAL STRENGTH-BASED GEOLOCATION

DISSERTATION

Amanda Sue King, Civilian

AFIT–ENG–DS–13–J–02

DEPARTMENT OF THE AIR FORCE
AIR UNIVERSITY

AIR FORCE INSTITUTE OF TECHNOLOGY

Wright-Patterson Air Force Base, Ohio

The views expressed in this dissertation are those of the author and do not reflect the official policy or position of the United States Air Force, the Department of Defense, or the United States Government.

AFIT–ENG–DS–13–J–02

DEVELOPMENT OF A MODEL AND LOCALIZATION ALGORITHM FOR RECEIVED SIGNAL STRENGTH-BASED GEOLOCATION

DISSERTATION

Presented to the Faculty

Graduate School of Engineering

and Management

Air Force Institute of Technology

Air University

Air Education and Training Command

in Partial Fulfillment of the Requirements for the

Degree of Doctor of Philosophy

Amanda Sue King, B.S., M.S.

Civilian

June 2013

AFIT–ENG–DS–13–J–02

DEVELOPMENT OF A MODEL AND LOCALIZATION ALGORITHM FOR RECEIVED SIGNAL STRENGTH-BASED GEOLOCATION

DISSERTATION

Amanda Sue King, B.S., M.S.
Civilian

Approved:

Richard K. Martin, Ph.D. (Chairman)	Date
Maj. Ryan W. Thomas, Ph.D. (Member)	Date
Michael A. Temple, Ph.D. (Member)	Date
Mark E. Oxley, Ph.D. (Member)	Date

Accepted:

HEIDI R. RIES, Ph.D. Interim Dean, Graduate School of Engineering and Management	Date

AFIT–ENG–DS–13–J–02

Abstract

Location-Based Services (LBS), also called geolocation, have become increasingly popular in the past decades. They have several uses ranging from assisting emergency personnel, military reconnaissance and applications in social media. In geolocation a group of sensors estimate the location of transmitters using position and Radio Frequency (RF) information. A review of the literature revealed that a majority of the Received Signal Strength (RSS) techniques used made erroneous assumptions about the distribution or ignored effects of multiple transmitters, noise and multiple antennas. Further, the corresponding algorithms are often mathematically complex and computationally expensive. To address the issues this dissertation focused on RSS models which account for external factors effects and algorithms that are more efficient and accurate.

The models of RSS that were developed in this research include a multiple transmitter model, a multiple antenna model and several models using Differential Received Signal Strength (DRSS). A DRSS model produced results that were 80% more accurate when compared with a traditional path-loss RSS model for localization of multiple transmitters.

The principal contributions of this research to the community include new models for RSS and two novel algorithms used to localize RSS measurements. These contributions also included development of DRSS models and algorithms that have not previously been seen in the literature.

To my Mom and in memory of my Dad.

Acknowledgments

First and foremost, I would like to express my gratitude to my advisor, Dr. Richard Martin, for giving me this opportunity. I could not have completed this dissertation without his help and guidance. Additionally, I would like to thank Dr. Ryan Thomas for all of the tele-conferences in which he has participated and all of the drafts he has corrected. I also would like to express my appreciation to Dr. Mark Oxley and Dr. Michael Temple for wonderful teaching and for serving on my committee. A big thank you goes to Jason Pennington and Russell Lenahan for their assistance with data collection.

Amanda Sue King

Table of Contents

Page

Page

List of Figures

List of Tables

List of Acronyms

Acronym	Definition
AFIT	the Air Force Institute of Technology
AOA	Angle of Arrival
AWGN	Additive White Gaussian Noise
CLT	Central Limit Theorem
CRLB	Cramer Rao Lower Bound
DRSS	Differential Received Signal Strength
EM	Expectation Maximization
GMM	Gaussian Mixture Model
LBS	Location-Based Services
MLE	Maximum Likelihood Estimation
NeSh	Network Shadowing
NLOS	Non-Line-of-Sight
PDF	Probability Density Function
PSD	Power Spectral Density
RF	Radio Frequency
RFID	Radio Frequency Identification
RMSE	Root Mean Squared Error
RSS	Received Signal Strength
SSSD	Stationary Signal Strength Difference
TDOA	Time Difference of Arrival
TOA	Time of Arrival
WA	Weighted Average
WLS	Weighted Least Squares

DEVELOPMENT OF A MODEL AND LOCALIZATION ALGORITHM FOR RECEIVED SIGNAL STRENGTH-BASED GEOLOCATION

I. Introduction

Location-Based Services (LBS) have become increasingly more important over the past few decades. According to Pyramid Research, revenue from LBS is expected to increase from two billion USD in 2010 to an expected 10.3 billion USD by 2015 [1]. With such an expected increase in the revenue from these services, there is a significant need to expand and examine current methods that are used in source localization.

1.1 What is geolocation and who uses it?

Applications of LBS include locating a transmitter to assist in billing services, providing assistance to emergency personnel, or performing military reconnaissance. A new and emerging area of geolocation is social media. For example, in applications such as Facebook, Four Square and Instagram, users may choose to tag their locations in status updates or photos. These applications collectively use what is referred to as geolocation, or more commonly "source localization" to execute these tasks.

Geolocation is the process of estimating the location of an unknown source or "transmitter" using a collection of measurements obtained from sensors or "receivers". In geolocation a group of sensors or "receivers" estimate the location of an unknown source or "transmitter" using position and Radio Frequency (RF) information. In order to use geolocation, sensors must be able to locate the origin of the signal. When the position of the source is unknown, localization techniques must be employed. A variety of different techniques can be used in geolocation.

1.2 How is geolocation performed?

Several different techniques are commonly used for RF geolocation including, Time Difference of Arrival (TDOA), Time of Arrival (TOA), Angle of Arrival (AOA) and Received Signal Strength (RSS). The TDOA, AOA and TOA estimation procedures generally require a larger number of operations due to their mathematical complexity and may be more hardware intensive than RSS measurements. For this reason, this research focuses on RSS as the measurement to locate transmitters. The RSS may be obtained from a variety of different sources and is defined as the amount of power present in a radio signal, or the power level being received by the antenna. Once RSS measurements are obtained from a receiver, a localization algorithm must be employed in order to utilize these estimates for source localization.

One new and emerging field of source localization uses Differential Received Signal Strength (Differential Received Signal Strength (DRSS)) measurements which are essentially the difference in RSS measurements at receivers. This is a convenient method for localization, since it alleviates the assumption of transmit power. Since DRSS measurements use in localization is a relatively new topic, Chapter 5 of this dissertation is dedicated to the development and analysis of DRSS models and algorithms.

There are several varying localization algorithms in the literature each associated with different RSS models. Sometimes closed-form approximation solutions are available for the estimation of the location. However, these are generally very mathematically complex, and involve approximations that can lead to error. Often, iterative algorithms must be performed in order to localize the transmitter and several of these algorithms are explored in this research.

1.3 Why is this research important?

The current literature on RSS-based geolocation is extensive and encompasses a variety of models, algorithms and experiments. However, since most current literature

relies on statistical models, questions arise as to the validity of the models and assumptions made.

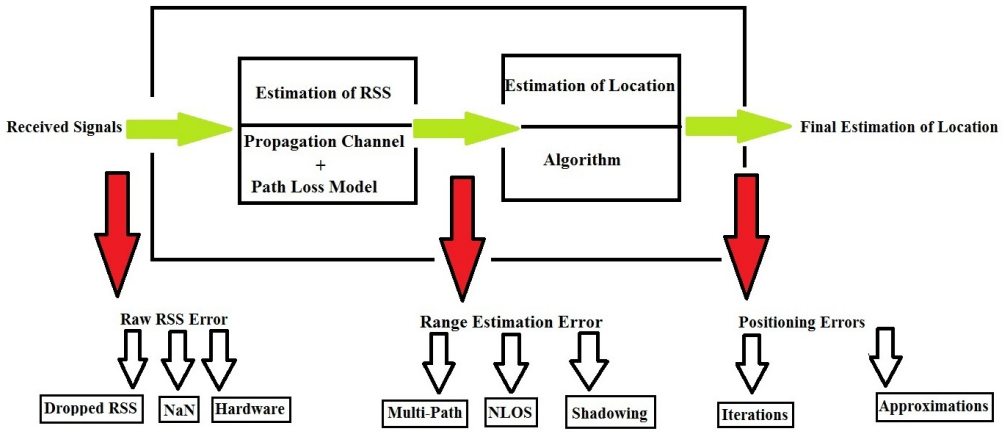

Figure 1.1: Potential sources of error in RSS localization process.

This research focused on investigating and alleviating errors associated with the localization process and each chapter relates to these errors. Figure 1.1 identifies three main areas in which error can be introduced into the localization process and this provides motivation for the bulk of this dissertation. These three main areas include raw RSS measurements, range estimation error, and positioning error. Range estimation errors are introduced into RSS measurements by way of multi-path, Non-Line-of-Sight (NLOS) obstructions and shadowing. All of these introduce error into the RSS measurements. Different models have been proposed to mitigate these errors. Known models as well as this author's original models are discussed in Chapter 2.

Raw RSS errors are caused by deficiencies in the hardware. These deficiencies are either due to human, hardware or software issues. These deficiencies can result in RSS measurements which are dropped (not reported), or reported incorrectly. Chapter 3 presents

a novel approach to analyzing two hardware devices for their consistency in reporting RSS measurements.

Positioning errors can result if restraints are put on the number of iterations that need to be run for a localization algorithm to converge. Several localization algorithms have been purposed in an attempt to minimize positioning error while maximizing the efficiency of the algorithm. These new algorithms along with simulations and validations can be found in Chapters 4 and 5.

1.4 What are the main contributions of this work and where are they located?

Below is a list of the major contributions of this dissertation.

1. Hardware was analyzed for performance in reporting consistent RSS measurements. These raw measurements were then used to validate the performance of the proposed algorithms. A novel way to compare raw RSS measurements from hardware was also presented. This can be found in Chapter 3.

2. This research proposes several new RSS models: (1) correlated RSS, (2) correlated DRSS, (3) multiple transmitter DRSS, (4) cooperative RSS, (5) non-cooperative RSS and (6) multiple antenna RSS. The author's original models were, Gaussian Mixture Model (GMM), RSS and multiple transmitter DRSS. The other models were variations on models that were already available in the literature. These models can be found in Chapter 2.

3. This research analyzes existing algorithms using the new proposed models and proposed some novel algorithms for localization: (1) GMM Maximum Likelihood Estimation (MLE), (2) non-cooperative and (3) cooperative MLE and (4) multiple transmitter MLE. It also compared existing algorithms with regard to accuracy. In this chapter the transmit power is assumed to be known. All of these algorithms can be found in Chapter 4.

4. This research proposes a new measurement (DRSS) of RSS with which to localize one or more transmitters, including the multiple transmitter DRSS and the correlated DRSS models. Localization algorithms were developed using these models: (1)DRSS gradient descent, (2) DRSS grid-search and (3) multiple transmitter DRSS. This can be found in Chapter 5. In this chapter the transmit power is assumed to be unknown.

This dissertation is organized as follows. Chapter 2 is a review of current RSS models that were compared in this research and new RSS models that were developed. Chapter 3 provides an analysis of RSS measurements obtained from a variety of hardware and then compares current and proposed models using this raw data. Chapter 4 gives a background on some currently used localization algorithms for which transmit power is assumed known and provides new algorithms that were developed in the course of this research. Chapter 5 gives the development of a new DRSS model which does not assume that transmit power is known as well as new localization algorithms that were developed or used with this model. Finally, Chapter 6 summarizes this research, gives ideas for future work and lists current and pending publications.

II. RSS Model Development

2.1 Parameters and chapter organization

This chapter will briefly discusses common RSS models and then discusses new models that were developed in the course of this research. It begins with common variations on the path-loss model and provides references for these models. A model which considers multiple receiving antennas is developed, followed by a model which uses non-cooperative measurements. Non-cooperative measurements are those where the signal cannot be demodulated from the noise. Finally, a model which has multiple transmitters is shown. This chapter provides the background for the algorithm development found in later chapters.

Unknown parameters and assumptions are shown in Table 2.1 on page 7 and known parameters are found in Table 2.2 on page 8. When using RSS for geolocation, the unknown parameter is the location of the transmitter(s), $(x_m, y_m) \in \mathbb{R}^2$ related to a fixed coordinate system (which is sometimes expressed as a complex value, $z_m = x_m + i \cdot y_m$).

2.2 Noise free path-loss RSS model

This section begins with a discussion of path-loss RSS models and variations of these models. Many authors state that a simple propagation model may be used to model RSS [2], [3], [4]. The simple radio propagation model assumes the signal strength is inversely proportional to the distance between the transmitter and the receiver. RSS is commonly given in dB, which suggests that distance measurements should be expressed in dB. The noise-free RSS model [5], is given by

$$r_s = P_0 - 10\eta log_{10}\left(\frac{d_s}{d_0}\right), \tag{2.1}$$

Table 2.1: Unknown parameters and assumptions

Symbol	Description	Standard Definition
$\mathbf{r}$	RSS measurement w/o noise (log)	$\mathbf{r} = P_0 - \eta \log_{10}(\mathbf{d})$
$\tilde{\mathbf{r}}$	Differential RSS w/o noise	$\tilde{\mathbf{r}} = \mathbf{A}\mathbf{r}$
$\mathbf{p}$	RSS measurements (log)	$\mathbf{p} = P_0 - \eta\bar{d}_s + \mathbf{w}$
$(x_m, y_m) = z_m$	True location of the m^{th} Tx	Varies
$\mathbf{q}$	DRSS w/ noise	$\mathbf{q} = \mathbf{A}\mathbf{p}$
w_s	Noise Fading for RSS at sensor s	$w_s \sim N(\mathbf{0}, \mathbf{\Sigma})$
$\mathbf{A}$	Matrix to constrain RSS measurements	$[\mathbf{1}_{(S-1)\times 1}, -\mathbf{I}_{(S-1)\times(S-1)}]$
v_s	Correlated noise in DRSS	$v_s \sim N(\mathbf{0}, \mathbf{A\Sigma A}^T)$
p_{coop}	Cooperative RSS measurements	$\begin{cases} p_s, & p_s \geq \tau_{coop} \\ Not\,a\,Number, & p_s < \tau_{coop} \end{cases}$
R_{sm}	Multiple Tx RSS w/o noise (linear)	$R_{sm} = P_0\left(\frac{d_0}{d_s(z_m)}\right)^{\eta}$
P_s	Multiple Tx RSS w/ noise (linear)	$P_s = \sum_{m=1}^{M} R_{sm} 10^{w_{sm}/10}$

where r_s is the RSS of receiver s, in dB, P_0 is the dimensionless constant transmit power of the single transmitter, η is the path-loss exponent for all sensors, d_s is the distance from the transmitter to receiver s in meters, and d_0 is the close-in reference distance generally taken to be one meter. Equation (2.1) forms the basis for investigation of RSS models in this research and all future models are fundamentally variations on (2.1). Expressed in a linear scale, the noise-free RSS or received power at the transmitter is,

$$R_s = \bar{P}_0\left(\frac{d_0}{d_s}\right)^{\eta}, \tag{2.2}$$

where $\bar{P}_0$ is P_0 expressed in linear terms as the transmitted power, d_s is the distance between the transmitter and receiver s and η is the path-loss exponent (the rate at which the signal decays) across all receivers. Most measurements of RSS are obtained in dB. However,

Table 2.2: Known parameters and assumptions

Symbol	Description	Standard Definition
M	Known number of transmitters	1 to 3
N	Known number of antennas	1 to 2
S	Known # of receivers	4 to 400
s	Index to indicate receiver	$s \in \{1, 2, \cdots, S\}$
m	Index to indicate transmitter	$m \in \{1, 2, \cdots, M\}$
n	Index to indicate antenna	$n \in \{1, 2, \cdots, N\}$
P_0	Constant transmit power	20 dB
g_0	Antenna 1 gain	0 dB
g_1	Antenna 2 gain	-10 dB
η	Path-loss exponent	$1 \leq \eta \leq 4$
σ	RSS standard deviation	$4dB \leq \sigma \leq 12dB$
$(x_s, y_s) = z_s$	Known location of receivers	$z_s = x_s + iy_s$
d_0	Close-in reference distance	1 meter
d_s	Distance from Tx to Rx, s position.	$\lvert z_s - z_m \rvert$
$\bar{d}_s$	Distance in log terms.	$10\log_{10}(d_s)$
ϖ_n	Gaussian mixture weight	$\varpi_n \in [0, 1] \; \forall \, n \in \{1, \cdots, N\}$
ρ	Correlation coefficient	$0.2 \leq \rho \leq 0.8$
τ_{coop}	Lowest signal RSS detected in noise	-40 dB

(2.2) forms the basis for other models in this research so it is important to understand the relationship shown in (2.2).

Equation (2.1) can be thought of as an ideal situation. There is no noise or fading assumed in the channel and generally, P_0 and d_0 are assumed to be known or easily

obtained. Even in an open field, RSS signals may still suffer from fluctuations and can induce errors in the form of shadowing and multi-path to the measurements. Therefore, it is important to introduce a variable to account for noise fading into the model.

2.3 Noise-added path-loss RSS model

Noise is defined as the variation in the amount of fading that occurs in RSS measurements due to obstacles in the path of the signal and it is not RF noise [6], [7], [8], [9]. It is common to include a term in (2.1) to account for noise in this model w_s,

$$p_s = P_0 - 10\eta log_{10}\frac{d_s}{d_0} + w_s \tag{2.3}$$

where P_0 is the constant transmit power in dB, d_s is the distance from receiver s to the transmitter, d_0 is the close-in reference distance and w_s is the noise, which is Gaussian in the log domain with zero mean and variance $\sigma^2 > 0$. Typically σ^2 is defined as the variance of noise introduced to the channel by multi-path, fading, shadowing, and Non-Line of Sight (NLOS), all previously discussed sources of error. Equation (2.3) does not specifically account for any external factors that may affect the quality of the signal but rather uses w_s to account for all noise in the model and assumes that noise measurements are independent from one another and, thus, uncorrelated. The next section explores correlation among noise terms.

2.4 Spatially-correlated noise fading RSS model

Making assumptions that are incorrect with regards to noise in the channel will add error to the model for received signal strength. It is less common in the literature to assume that RSS measurements are correlated, but this does not mean it is not important. Not accounting for dependence of noise fading terms misrepresents the accuracy of the location estimate.

This research introduces using correlated noise fading measurements to derive a RSS model. Here, the assumption is made that the correlation occurs in the noise not in the

path-loss terms. Path-loss is assumed to be constant across all receivers. When considering (2.1) with respect to correlated noise fading, a model can be provided which accounts for correlated noise fading measurements.

Figure 2.1 is a pictorial representation of how correlation can occur in the noise fading. It shows that when paths A and B must pass through similar obstacles to reach the transmitter, there will likely be a large correlation between the measurements at A and B. Conversely, there would likely be a low correlation between A or B and C.

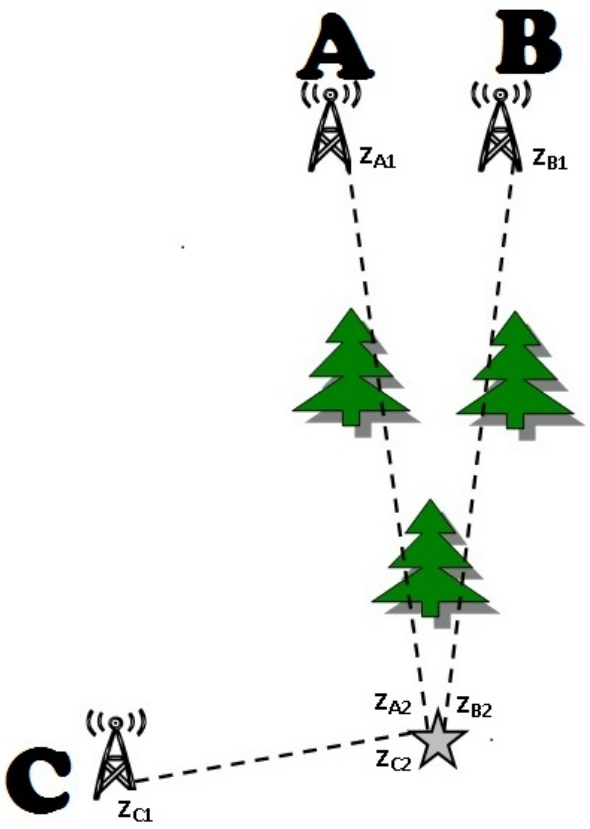

Figure 2.1: Example of spatial correlated shadowing. The signal transmitted by the star shaped node will experience different shadowing effects. It is expected that the shadowing at A and B to be highly correlated since the signals travel through the same environment and C to have a low correlation with either A or B.

2.4.1 Literature review of current correlated noise fading RSS models.

Gudmundson [10] presents one of the earliest correlated shadowing models, a simple decreasing correlation function, given by

$$\mathbf{\Sigma} = \sigma^2 \rho^{|s|} \tag{2.4}$$

$$\rho = \epsilon^{vT/d_s}, \tag{2.5}$$

where ϵ is the correlation between two points separated by distance d_s, v is mobile velocity, T is the integer number of seconds of a sample. Since the transmitters are stationary, this research uses constant velocity.

Flam et al. [11] use correlated RSS measurements to localize a source. They differ in their definition of correlation.

$$p_s = P_0 - 10\eta \log(||z_s - z_0||/d_0) + w_s \tag{2.6}$$

where (2.6) follows the form of (2.3), $w_s \sim N(\mathbf{0}, \mathbf{\Sigma})$, $||z_s - z_0||$ is the norm and

$$\mathbf{\Sigma}_{ms} = \sigma^2 e^{-d_{ms}/X_c}, \tag{2.7}$$

where X_c is the correlation distance (the authors do not explicitly state where the computation of X_c comes from), $\mathbf{0}$ is the zero matrix and $\mathbf{\Sigma}$ is the covariance matrix.

Al-Dhalaan and Lambadaris [12] estimate transmitter location using the popular Network Shadowing (NeSh) model to account for correlation in the measurements. Consider links between transmitter receiver pairs, as in Figure 2.1, where each point (A, B or C) has two coordinates. In order to determine the correlation between A and B, define endpoints of A to be z_{A1} and z_{A2} and endpoints of B to be z_{B1} and z_{B2},

$$Cov(A, B) = \frac{\sigma^2/\delta}{\sqrt{d_A}\sqrt{d_B}} \int_{z_{A1}}^{z_{A2}} \int_{z_{B1}}^{z_{B2}} \mathrm{e}^{-\frac{\|\mathbf{r}-\mathbf{p}\|}{\delta}} \mathrm{d}\mathbf{p}\, \mathrm{d}\mathbf{r}\,, \tag{2.8}$$

where $\delta > 0$ is a space constant, $d_A = |z_{A1} - z_{A2}|$, $d_B = |z_{B1} - z_{B2}|$ are the distances from points in A and B, respectively, and z_{A1}, z_{A2}, z_{B1}, z_{B2} are the endpoints of A and

B, respectively. Patwari and Agrawal [13] also use a NeSh model to model the effects of correlated shadowing. This is a mathematically complicated covariance model which requires multiple integrations to compute and for this reason was not considered in this research.

Assad et al. [14] utilize Radio Frequency Identification (RFID) technology for their real time experiment. Even though this is not directly applicable to this author's research, they do incorporate a correlated log normal shadowing term and then use positioning software to solve the model. They define a break point, d_{BP} at which the values of η and σ^2 change.

$$r_s = \begin{cases} 10\eta_1 \log_{10}(d_s), & d_s \leq d_{BP} \\ 10\eta_1 \log_{10}(d_{BP}) + 10\eta_2 \log_{10}\left(\frac{d_s}{d_{BP}}\right), & d_s > d_{BP} \end{cases} \tag{2.9}$$

where η_1 is the power-distance gradient before the breakpoint and η_2 after the breakpoint, and η_1, η_2 and d_{BP} are defined using the standard IEEE 802.11 channel model. Their definition of the fading correlation was

$$p_s = P_0 - r_s + w_s, \tag{2.10}$$

where $w_s = \rho w_{s-1} + \sqrt{1-\rho^2} \cdot N(0, \sigma)$ and $\rho = 0.96$ which is close to perfect correlation and may not accurately portray correlation effects.

2.4.2 Proposed correlated noise fading RSS model.

The amount of correlation in the noise fading can be accounted for by defining a correlation coefficient ρ [10, 15, 16]. Research in the field of correlation noise fading of RSS measurements is supported by previous endeavors from the authors mentioned above.

The goal of this dissertation is to find a model which takes less operations to compute and is not mathematically complicated. Therefore, this author's model considers a simple correlated shadowing model as opposed to some of the other models that are described

above, since it is desirable to use a model that will minimize additional error that might be introduced with a more complicated model.

This author defines correlated fading noise, w_s to be a random vector, from a Gaussian distribution with mean zero and covariance matrix, $\mathbf{\Sigma}$, defined as σ^2 along the diagonal and $\rho\sigma^2$ on the off-diagonal matrix. A particular correlation fading model is assumed for analytical purposes only. Theoretically, any other correlation model could be used. For simplicity all ρ values are the same, but could be varied to fit other models.

If noise fading is spatially correlated, a matrix is defined to account for the amount of correlation in the noise fading terms,

$$\mathbf{\Sigma} = \sigma^2 \left(\rho \mathbf{1}_S \mathbf{1}_S{}^T + (1-\rho)\mathbf{I}_S \right), \tag{2.11}$$

where, ρ is the correlation coefficient for the noise measurements, σ^2 is the amount of variance in the noise, $\mathbf{1}_S$ is an $S \times 1$ matrix of ones, $\mathbf{I}_S$ is an $S \times S$ identity matrix, and S is the number of receivers. Transpose of a matrix A is denoted as A^T. This is the standard notation that will be used in the rest of this dissertation. Using (2.11), a spatially correlated noise fading model for RSS is,

$$\begin{aligned} \mathbf{p} &= \mathbf{r} + \mathbf{w} \\ &= P_0 - 10\eta \log_{10}(d_s) + w_s, \end{aligned} \tag{2.12}$$

where $\mathbf{r}$ is the noise free path-loss model from (2.1), $\mathbf{d}$ is a vector of distances from the transmitter to each receiver, P_0 is the constant transmit power and $\mathbf{w} \sim N(\mathbf{0}, \mathbf{\Sigma})$ is the correlated noise fading. In the remainder of the paper, the simple correlated fading model for RSS is defined by (2.11) and (2.12).

2.5 Single transmitter with multiple antenna RSS model (RSS-GMM)

Several factors may affect the distribution of RSS measurements. As mentioned previously, measurements may be affected by terrain, software, environment and hardware

configurations. These are all important factors to consider when trying to find an appropriate model for a distribution of RSS values.

2.5.1 A review of the literature of current non-Gaussian RSS models.

As mentioned previously, the localization of a transmitter with multiple antennas is generally modeled as a single received signal coming from a Gaussian distribution [9]. While the standard log-distance path-loss model is often used to model RSS, it is not always the optimal choice. Much current research considers transmitters to have a single omni-directional antenna, although this is not always the case. Often transmitters may have two or more antennas. Most models assume a Gaussian distribution and do not consider the number of antennas. Error that is introduced into the model by these incorrect assumptions is investigated in this research. Kaemarungsi et al. [17] suggest that the distribution of RSS may not be normally distributed and may be affected by the presence of a user's body. Most of the experiments they performed showed that RSS did not fit the Normal distribution and tended to be left skewed.

Patwari et al. [18] ran a Kolmogorov-Smirnov (KS) test to confirm that at a rejection level of $\alpha = 0.10$, the distribution of RSS measurements they observed when using multiple transmitter antennas were more closely modeled by using a Gaussian Mixture Model (GMM) and the null hypothesis test for a GMM distribution was not rejected. There was insufficient evidence to conclude that the shape of their data did not come from a GMM distribution.

Sheng et al. [19] propose that when multiple transmitters antennas are used to achieve antenna diversity, the received signal strength (RSS) may be modeled as a GMM in the dB domain.

Antenna diversity may also be used in the localization of a transmitter when receiver locations are known. Figure 2.2 shows an example of antenna diversity. Two antennas spaced a few wavelengths apart transmit signals at different strengths due to interferences

from reflections, fading or line-of-sight. Thus, for any set of RSS measurements, a distribution which contains several different Gaussian distributions, each with unique mean and known standard deviation, may be seen.

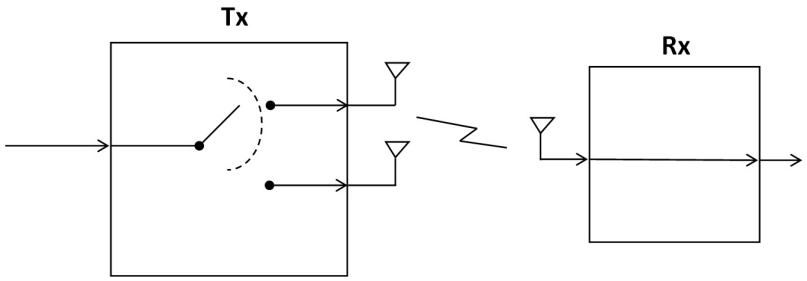

Figure 2.2: Example of antenna diversity, utilized by a transmitter, with $M = 2$ antennas.

2.5.2 Proposed single transmitter multiple antenna RSS model.

This research developed a GMM to model RSS coming from multiple receivers to a transmitter with multiple antennas. A GMM model is attractive in this research, because it can account for Gaussian signals from multiple antennas and has been shown to accurately model signals using antenna diversity [18], [19].

The variable w_s, accounts for the shadow fading between the transmitter and receiver and is known to be modeled as a Gaussian random variable with zero mean and known standard deviation σ^2.

The model makes the following assumptions:

1. A log-distance path-loss model is used.
2. There are two omni-directional antennas located at a single transmitter, however, only one is used at a time and they have different antenna gains (g_1, g_2).
3. Noise for each antenna is modeled as coming from an Additive White Gaussian Noise (AWGN) channel.
4. Receiver locations are known.

Equation (2.1) is the generally accepted form for the path-loss model without fading, but may not accurately model signals from a transmitter with multiple antennas utilizing antenna diversity. When two antennas are present at the transmitter, each is contributing an unknown amount of power, which can represented by two Gaussian distributions.

$$\bar{r} = \begin{cases} r + g_1, & \textit{with probability } p_1 \\ r + g_2, & \textit{with probability } p_2 \end{cases} \tag{2.13}$$

where r is RSS measurements without noise at antenna $n = 1$ or 2 and g_1 and g_2 are the gains of the two transmitter antennas. There is an equal chance of the signal coming from either antenna. Note, for this research only two antennas were considered, but theoretically any number of antennas could be considered. Using a predetermined weight a Probability Density Function (PDF) may be found which specifies the GMM. For a single Gaussian variable the PDF is

$$f(\mathbf{p}; \bar{\mathbf{r}}) = \int_{-\infty}^{\infty} \frac{1}{\sqrt{2\pi\sigma^2}} \exp\left[-\frac{\|\bar{\mathbf{r}} - \mathbf{p}\|^2}{2\sigma^2}\right] \mathrm{d}\mathbf{r} \,, \tag{2.14}$$

where variance σ^2 is known, $\mathbf{p}$, $\bar{\mathbf{r}}$ are mean RSS as defined in (2.13) and (2.1), respectively. When utilizing antenna diversity, the transmitter chooses the signal from the strongest antenna reading. Assume that approximately $100/N\%$ of the time the signals come from antenna n, then (2.14) may be combined with the weights ϖ_n, to form a sum of n weighted Gaussians, each with its own unique mean.

$$f(p; \bar{r}) = \sum_{n=1}^{N} \varpi_n f(p_n; \bar{r}) \tag{2.15}$$

where N is the number of antennas, ϖ_n is the weight associated with the n^{th} antenna and p_n is the mean associated with the n^{th} mixture. Using (2.15), a MLE was found which maximizes the log-likelihood function and is discussed in Section 4.6.

2.6 Cooperative and non-cooperative RSS models

Most current models assume measurements are obtained cooperatively. This means that the signal is known and can be demodulated from the noise. RSS measurements also

suffer from range limits. Both of these ideas formed the basis for a research paper. This author's research has involved another type of model, non-cooperative. A non-cooperative model is defined as one for which the signal is not demodulated. Since integrating the Power Spectral Density (PSD) is mathematically complex, an approximation may be used as defined in [6].

"In a non-cooperative system, such as locating emitters in a hostile environment, the RSS may be determined by integrating the observed Power Spectral Density (PSD)."

It is shown that the standard model becomes invalid for this case at large distances. This is the basis for trying to derive a model for RSS which accounts for a non-cooperative system. Traditional models which fail to account for a noise floor in their measurements are over confident in their use. In reality, the actual power measurements will exhibit a leveling off at the noise floor. This is another important aspect of modeling RSS which will be considered in this author's research.

2.6.1 Development of a cooperative model RSS model (RSS-NC).

In a cooperative system, range limits may be approximated via a truncation function. Using a simple path-loss propagation model and considering the power of the noise, the RSS in dBm may be modeled as,

$$p_{coop} = \begin{cases} p_s, & p_s \geq \tau_{coop} \\ NaN, & p_s < \tau_{coop} \end{cases}, \tag{2.16}$$

where NaN means "not a number" and indicates that no RSS was reported, p_s is the received power after fading as modeled by (2.3) and τ_{coop} is the lowest signal RSS that can be detected in the presence of noise.

2.6.2 Literature review of non-cooperative RSS model.

Chang-Young et al. [20] propose a measurement of RSS without prior knowledge of the locations of the sensors or transmitters. Additionally, they hypothesize that path-loss

and constant transmit power both vary. The resulting model is shown below,

$$p_s = r_s + w_s \tag{2.17}$$

$$r_s = P_s - 10\eta log_{10}(d_s) \tag{2.18}$$

$$r_{coop} = \begin{cases} r_s, & if \quad r_s > \tau_{nc} \\ \tau, & O.W. \end{cases}, \tag{2.19}$$

where $\mathbf{w} \sim N(\mathbf{0}, \sigma^2\mathbf{I})$, P_s is the source power level and is unknown and r_s is the sensed RSS measurement. If the sensed RSS measurements are above a threshold (τ), then the RSS is as modeled in (2.18) with the addition of noise. However, if it is below the threshold, it is modeled as the threshold plus noise. Thus, if all of the RSS sensed are above a certain threshold, then the simulated RSS will be modeled using a standard log normal fading model. It appears to be similar to the cooperative model of (2.16), except instead of reporting NaN, the receiver reports the threshold for values below that threshold.

2.6.3 Development of non-cooperative RSS model (RSS-NC).

The non-cooperative model imposes a noise floor to the measurements as only measurements below the τ_{coop} are capable of being reported. Since the noise power is additive in the linear domain, it will be modeled as shown in (2.20). For a non-cooperative system there is a noise floor which must be incorporated into the RSS measurements.

$$\mathbf{p}_{nc} \sim \mathcal{N}(r_{nc}, \sigma^2\mathbf{I}) \tag{2.20}$$

$$r_{nc,s} = 10\log_{10}\left(10^{r_s/10} + 10^{\tau_{nc}/10}\right) \tag{2.21}$$

where r_{nc} is the non-cooperative power of the signal with addition of the power of the background noise, r_s is the power of the signal as found in (2.1) and τ_{nc} is the power of the background noise.

2.7 Multiple transmitter RSS model (RSS-M)

Simulations as reported by Nelson et al. [21] were recreated to test the accuracy of the author's proposed algorithm for estimating multiple transmitters' locations using multiple

receiver power measurements. Unknown transmitter locations are randomly drawn from a uniform distribution. The number of transmitters is known and they are assumed to have the same constant transmit power. The number of receivers is also known and their locations are again drawn randomly from a uniform distribution. Also, the number of receivers is at least twice the number of transmitters. The locations are estimated under a log-normal shadowing model, which has been validated to represent the variations in received power due to obstacles in the signal path [21]. The final location estimation is chosen as the estimate which maximizes the probability that the transmitters are correctly located given the observed power measurements at the receivers. Most research currently focuses on RSS measurements coming from a single transmitter. There may be opportunities to use multiple transmitter readings and the more data that is available the more accurate the estimates.

2.7.1 Development of multiple transmitter RSS model (RSS-M).

Throughout this section, a lower case letter denotes a term in dB and a capital letter represents a linear term. The power measurements are obtained by simulating the power at each transmitter using the following equation,

$$R_{sm} = P_0 \left(\frac{d_0}{d_s(z_m)} \right)^{\eta}, \tag{2.22}$$

where R_{sm} denotes the power received from a single transmitter to a single receiver: $d_s(z_m)$ is the distance from transmitter m to receiver s, P_0 is the constant transmit power, d_0 is the close-in reference distance generally taken to be one meter and η is the path-loss exponent. The power at receiver s, when w_s is a sample from a Normal distribution with variance equal to σ^2

$$P_s = \sum_{m=1}^{M} R_{sm} 10^{w_{sm}/10}, \tag{2.23}$$

where $w_{sm} \sim N(0, \sigma^2)$ is the noise in the signal, R_{sm} is the noise free power from receiver s to transmitter m, and P_s is the normalized sum of the power from receiver s to the

transmitter m. Note that (2.23) is expressed in linear terms

$$p_s = 10\log_{10}(P_s)\ , \tag{2.24}$$

where p_s is the model for power expressed in decibels. This chapter discusses the majority of the models used in this literature review with the exception of DRSS modeling. Chapter 5 discusses the extensive research for DRSS modeling. New models for RSS were explored. These models were (1) cooperative RSS, (2) non-cooperative RSS, (3) multiple antenna RSS and (4) correlated RSS and they were compared with the existing standard path-loss model.

Table 2.3 gives a summary of models used in this dissertation and the associated equation numbers of the model. The models shown in this table form the basis for algorithms that were derived in Chapters 4 and 5.

Table 2.3: Description of models used in the dissertation including their locations in this dissertation.

# of Tx	**Type**	**Fading Model**	**Equation**
1	RSS-STD (Standard)	No Noise	(2.1)
1	RSS-COOP (Cooperative)	Gaussian	(2.16)
1	RSS-NC (Non-Cooperative)	Gaussian	(2.20)
1	RSS-GMM (Gaussian Mixture Model)	Gaussian	(2.13)
1	RSS-CORR (Correlated)	Corr. Gaussian	(2.12)
1	DRSS-CORR (Correlated)	Diff. of Corr. Gaussians	(5.2)
M	RSS-M (Multiple Transmitters)	Gaussian	(2.23)
M	DRSS-M (Multiple Transmitters)	Diff. of Corr. Gaussians	(5.31)

III. Raw RSS Measurement Analysis

When the research for this dissertation first began the only equipment available for experiments were the SunSPOT sensor motes by Oracle. Research showed these motes to be ineffective and inaccurate. Therefore, additional hardware was purchased for use in experiments. This part of the dissertation compares the three sensor hardware platforms that were available for obtaining RSS measurements including Wi-Pry/WARP board combo, SunSPOT and Telos-B motes.

Most texts focus not on the raw RSS measurements but on a mean estimate of this data. Raw measurements coming to the receiver are not always constant and suffer from outages. In order to accurately model RSS measurements and have an understanding of where the signals originate from, an experimental campaign involving different hardware was first explored.

3.1 Motivation for investigation of external effects of error on RSS measurements

RSS measurements are obtained from a variety of different sources. Typically radio propagation is affected by multi-path which can be broken down into three components: reflection, diffraction and scattering. Reflection is generally caused by the surface of the earth, buildings or walls [7], [9]. Diffraction occurs when the waves must bend around an obstacle (caused by obstructions). Scattering of waves occur when objects that are smaller than the wavelength of the propagating wave are encountered, such as street signs and foliage. Figure 3.1 shows a pictorial representation of diffraction, scattering and reflection. All the properties shown in Figure 3.1 induce error into RSS measurements. Additionally, error may also be induced from users or equipment.

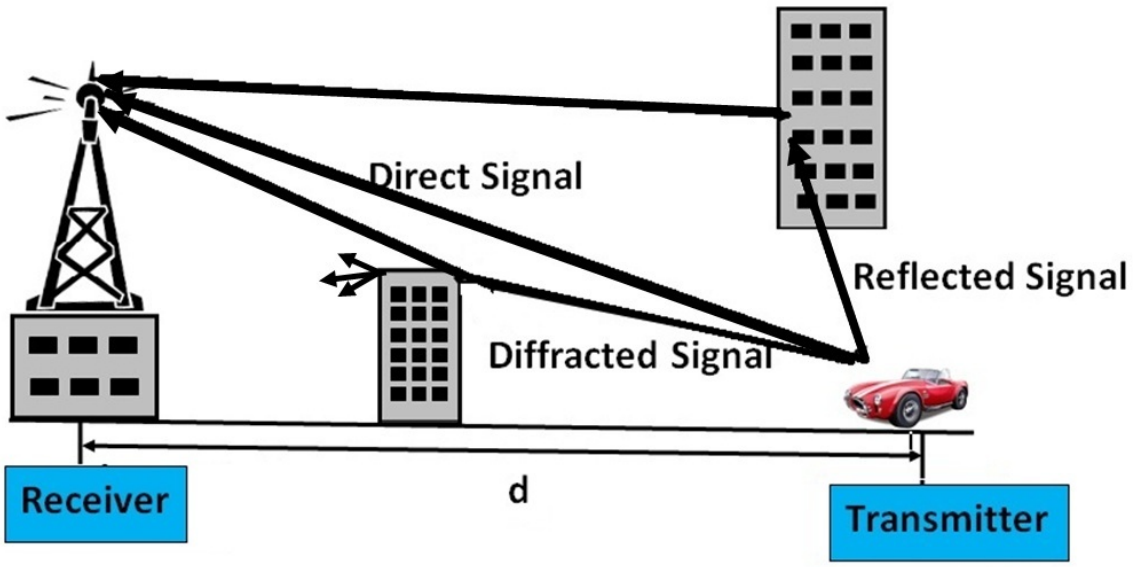

Figure 3.1: Example of reflection, diffraction and scattering that radio frequency waves experience when traveling through the air from a transmitter to a receiver.

3.2 RSS measurements obtained from SunSPOT motes

The measurements used to generate the results found in this section were performed at the Air Force Institute of Technology (AFIT), in an area that is relatively free of obstacles. Most current research focuses not on the raw RSS measurements but on a mean estimate of this data. Raw measurements coming to the receiver are not always constant and suffer from outages. Any calculations that involve these measurements are further affected by a wrong assumption about the raw data. In order to accurately model RSS measurements, it is important to first understand where raw data originates. An experimental campaign involving several different environments with RSS values will first be explored.

A transmitter was placed at the origin and sixteen receivers were placed around it at a radius of 14.5 feet, about every 22.5°, all in the same plane. Receivers were placed on poles which are three feet from the ground. Figure 3.2 shows the placement of the receivers and the transmitters.

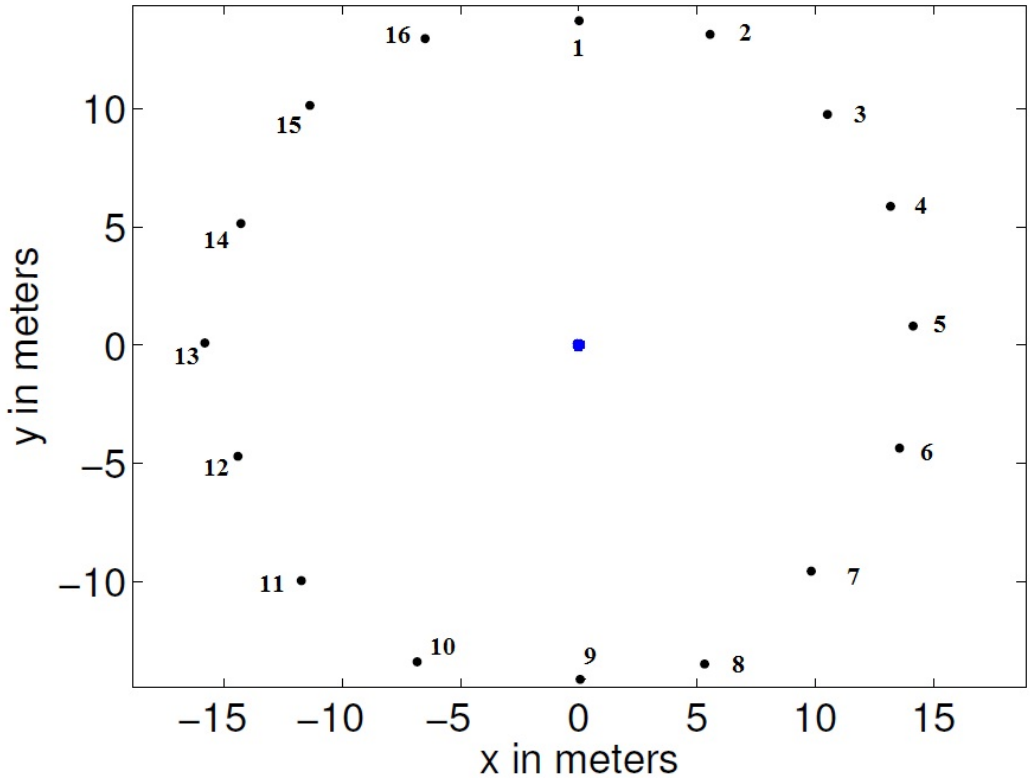

Figure 3.2: Receiver and transmitter placement for experiment which used the SunSPOT motes.

3.2.1 Initial data analysis of SunSPOT experiments.

Two sets of measurements were performed for this configuration, one right after another with the same exact setup and experimental conditions. Therefore, since the motes have omni-directional antennas, it is reasonable to assume that these measurements should come from similar distributions. Further, since the receivers are placed equidistant from the transmitter in a circular shape, it is reasonable to assume that they will all give similar RSS readings. The first step in any data analysis is to look at a graphical representation of the data. Figure 3.3 shows the distribution of all RSS measurements. Upon first inspection, the data does not appear to have the same shape. Table 3.1 gives the sample size, mean, median, standard deviation and number of *NaN*s reported for each experimental setup. During the experiment it was noted that some receivers reported outages, where no RSS

Table 3.1: Descriptive statistics for each experimental setup involving SunSPOT motes.

Experiment	**Sample Size**	μ	**Median**	σ	*NaN*s
A	10,832	-21	-20	5.6	5,221
B	10,816	-22	-21	7.1	5,330

measurement was reported. This is of particular interest and will be discussed later in this section. In this experiment, the number of *NaN* readings, which corresponds to an outage, are reported so that the reader may get a sense of the actual number of measurements that are used to calculate the mean, median and standard deviation.

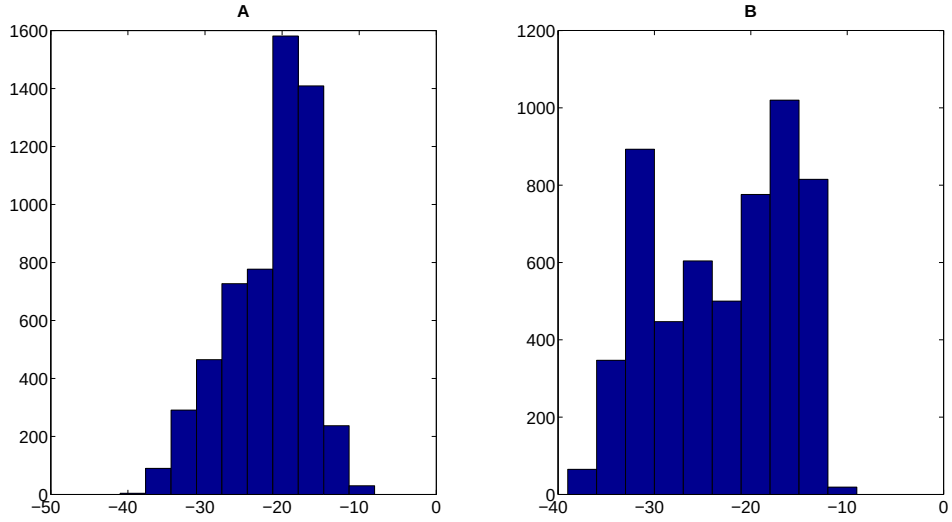

Figure 3.3: Distribution of RSS measurements obtained for circle geometry. Plot *A* is due to experiment one. Plot *B* is due to experiment two.

While the means appear to be similar, a statistical test is still warranted. Additionally, it will be beneficial to look at a time series plot for each receiver. This will help to identify outages in the data as well as to get a visual representation of the data. Due to the large number of graphs that were produced, only those with interesting patterns are shown in the text.

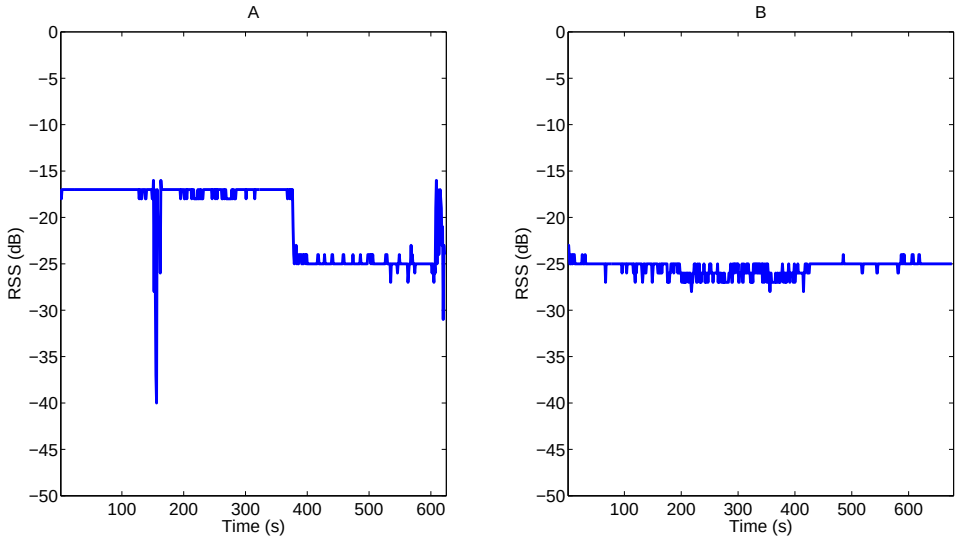

Figure 3.4: Raw RSS measurements coming from SunSPOTs for receiver in position five.

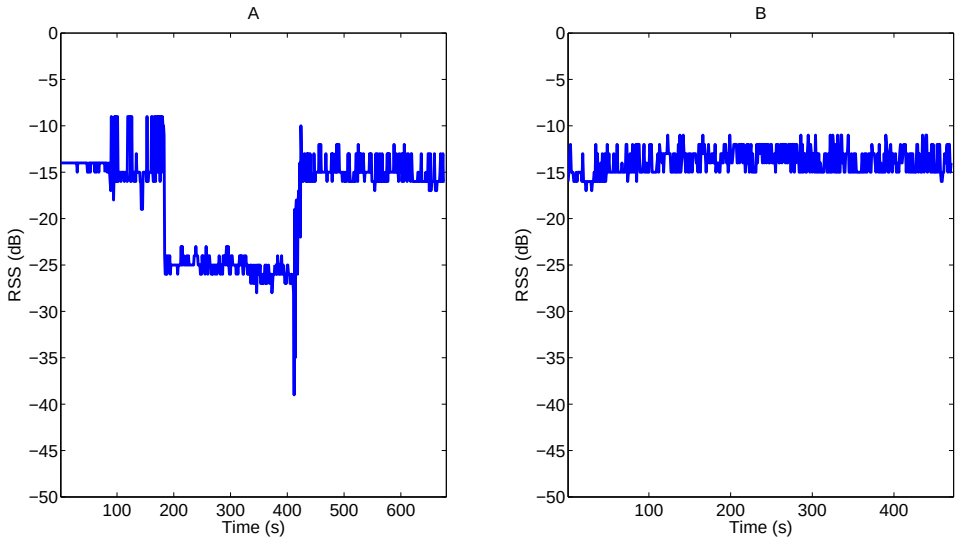

Figure 3.5: Raw RSS measurements coming from SunSPOTs for receiver in position six.

Figures 3.4 - 3.6 are found in a similar region on the circle of receivers, yet each produces markedly different time series plots. Since this was a controlled experiment, it is not expected to see such extreme drops as in Experiment A in Figures 3.4-3.6. Each of these receiver positions also reported generally uniform RSS values for Experiment B. It is hard

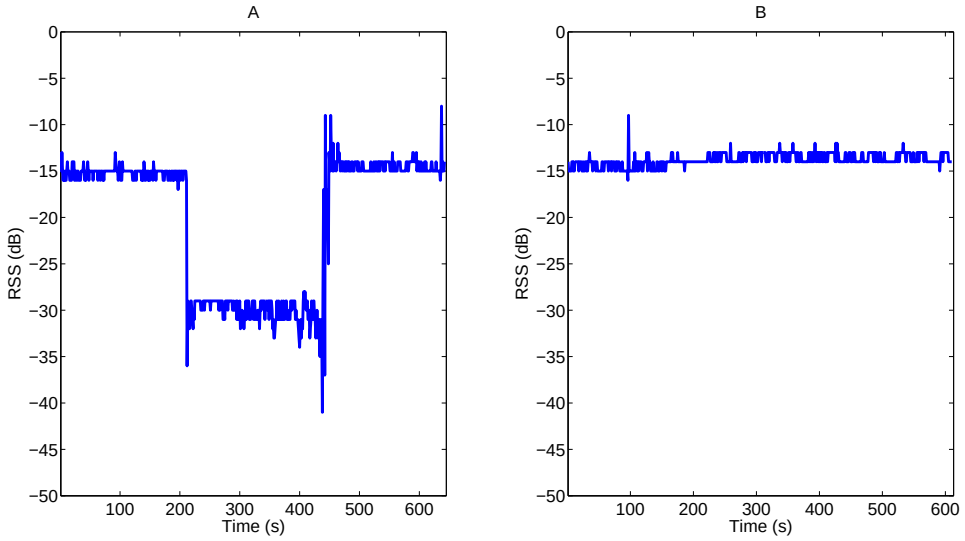

Figure 3.6: Raw RSS measurements coming from SunSPOTs for receiver in position seven.

to say for certain if there is a difference in this data. Further analysis will be needed and is discussed in the next section. Table 3.2 gives summary statistics for each receiver for both Experiment A and Experiment B. Receiver position, median, mean, standard deviation, and percentage of *NaN*s are shown and measurements were taken over a 676 second time interval. A measurement was reported once per second unless an outage occurred, in which case *NaN* was reported.

Interestingly, the receivers with the smallest amounts of outages, five, six and seven, show the most extreme differences between the two experiments, as shown in Figures 3.4-3.6. Further analysis will help show if significant differences exist between the two data sets.

3.2.2 T-test for consistency of SunSPOT data.

A T-test is used to look for differences in the mean RSS values for the two experiments performed on the SunSPOTs. Refer to [22] for a general description of T-tests. An important step prior to performing the T-test is to establish the significance level (α) and

Table 3.2: Descriptive statistics for all raw RSS measurements for two experiments involving SunSPOT motes.

Rx	$Median_1$	μ_1	σ_1	$NaNs_1$	$Median_2$	μ_2	σ_2	$NaNs_2$
1	-21	-21	0.36	47 %	-21	-21	0.18	46 %
2	-33	-33	1.4	78 %	-33	-33	1.3	84 %
3	-29	-29	4.9	59 %	-31	-32	2.0	32 %
4	-23	-24	1.9	45 %	-31	-31	0.91	38 %
5	-17	-20	3.9	8 %	-25	-25	0.73	0 %
6	-16	-18	5.4	0 %	-14	-14	1.4	30 %
7	-15	-20	7.4	5 %	-14	-14	0.69	10 %
8	-16	-16	0.61	50 %	-15	-15	0.57	46 %
9	-34	-34	0.85	87 %	-33	-33	0.81	57 %
10	-19	-19	0.61	69 %	-19	-19	0.60	66 %
11	-19	-19	0.55	50 %	-19	-19	0.43	46 %
12	-19	-19	0.72	50 %	-19	-19	0.66	74 %
13	-17	-17	0.52	81 %	-16	-16	0.58	64 %
14	-23	-23	0.40	49 %	-23	-23	0.70	80 %
15	-18	-18	0.46	49 %	-17	-17	0.16	76 %
16	-28	-28	0.89	45 %	-29	-29	0.70	40 %

calculate the degrees of freedom. The criterion used for rejecting the null hypothesis, α, is defined as the probability of a Type I error or "false positive". A Type I error would occur if it is concluded that the mean scores differ when they actually do not.

$$\alpha = P(Type\ I\ error) = P(Reject\ H_0 | H_0\ is\ true) \tag{3.1}$$

Here, P denotes the probability of a Type I error and $d.f. = n_1 + n_2 - 2$ is the degrees of freedom. The choice of a level of significance is not based on any mathematical, statistical or substantive theory. It is a choice which is purely arbitrary for our research since a cost cannot be attached to either a Type I or Type II error [23]. Thus, the significance level is set to $\alpha = 0.05$. The probability of a Type II error, β, is not generally used in analysis. However, the reader may refer to [24] for further explanation. A Type II error occurs if it is concluded that the mean scores do not differ when they actually do differ. The actual amount of variability in the sampling distribution of T depends on the sample size. This dependence is expressed by degrees of freedom ($d.f$). For each parameter being estimated a $d.f.$ is lost. Thus, when estimating two means, two degrees of freedom are lost.

Having established the initial parameters, the next step is to calculate the test statistic, T, and p-value. Decisions based on T-test results may be made by using either the test statistic (T) or the p-value. The T-statistic is the ratio of how much the data mean scores differ from each other by their total standard error. This is compared to a critical value, T_0, and a decision on whether to reject the null hypothesis is made if the T-statistic falls outside of the rejection region. T_0 may be found by looking at a standard T-table available in many statistics texts. The p-value or observed significance level is the probability of observing a value of the test statistic that is at least as extreme as the test statistic that was calculated from this data, assuming the null hypothesis is true [24]. When the null hypothesis is rejected, the result is said to be statistically significant. The T-test statistic and p-value are calculated using Equations (3.2) and (3.3) respectively.

$$T = \frac{\bar{x}_1 - \bar{x}_2}{\sqrt{\frac{s_1^2}{n_1} + \frac{s_2^2}{n_2}}} \tag{3.2}$$

$$p - value = P(|T| > T_0), \tag{3.3}$$

where $\bar{x}_i$ is the mean score of group $i, (i \in \{1, 2\})$, s_i^2 is the variance of data from group i, and n_i is the sample size of group i, with $n_1 = n_2 = 676$. With 674 degrees of freedom,

$\alpha = 0.05$ and $T_0 = 1.96$. The rejection region is, $T < -1.96$ or $T > 1.96$. For any value that falls outside of this region, reject the null hypothesis and conclude that there is a difference in the mean scores for the two groups.

Table 3.3 gives the corresponding receiver, T-statistics and p-values for the RSS values from the two experiments, respectively. The alternative hypotheses for all receivers would be $\mu_1 \neq \mu_2$. Here a two-sided hypothesis is used because the author is interested in any difference in the two groups.

As shown from the p-values, all null hypotheses except for receiver two may be rejected at an $\alpha = 0.05$ level. It can be concluded that there is a signficiant difference in the distributions of the RSS measurements taken from receivers 1 and 3-16. For receiver two, there is insufficient evidence to conclude that the two RSS measurements are from different distributions. This is surprising since it is expected that RSS measurements would be relatively similar for each set of measurements. This may be due to the large number of *NaN*s that were reported by the receivers. Focusing on the receivers at positions 5, 6 and 7, their T-statistic values can be interpreted. For receivers at position five, the positive nature of the T-statistic means that the mean RSS value for experiment A is larger than that of experiment B. At receiver positions six and seven, the negative nature of the T-statistic shows that the mean RSS measurements for experiment A are larger than that of experiment B. These results are puzzling and future analysis could involve looking into the nature and effects of missing measurements in these types of experiments. Numerous subsequent experiments produced similar results as seen here even when performed by a variety of different people, at a variety of different lengths and in a variety of environments in an attempt to produce usable data. Therefore, new motes (Telos-B) were obtained for use in order to continue conducting experiments.

This section showed the importance of testing equipment ahead of time when possible. If complete trust is put into the hardware without questioning consistency, then experiments

may produce erroneous results or lead to additional unnecessary testing. Experiments should be taken more than once if possible without varying conditions. Then those experiments should be compared to look for consistency in the measurements.

Table 3.3: T-test results for $H_0 : \mu_A = \mu_B$ versus $H_1 : \mu_A \neq \mu_B$, i.e. that the two experiments using SunSPOT motes have the same means or different means.

Receiver positions	**T-stat**	**p-value**
1	-8.44	< 0.0001
2	0.21	0.83
3	12.77	< 0.0001
4	62.65	< 0.0001
5	33.40	< 0.0001
6	-17.59	< 0.0001
7	-21.65	< 0.0001
8	-15.70	< 0.0001
9	-13.88	< 0.0001
10	5.31	< 0.0001
11	-4.97	< 0.0001
12	-7.04	< 0.0001
13	-17.72	< 0.0001
14	-8.09	< 0.0001
15	-27.18	< 0.0001
16	21.89	< 0.0001

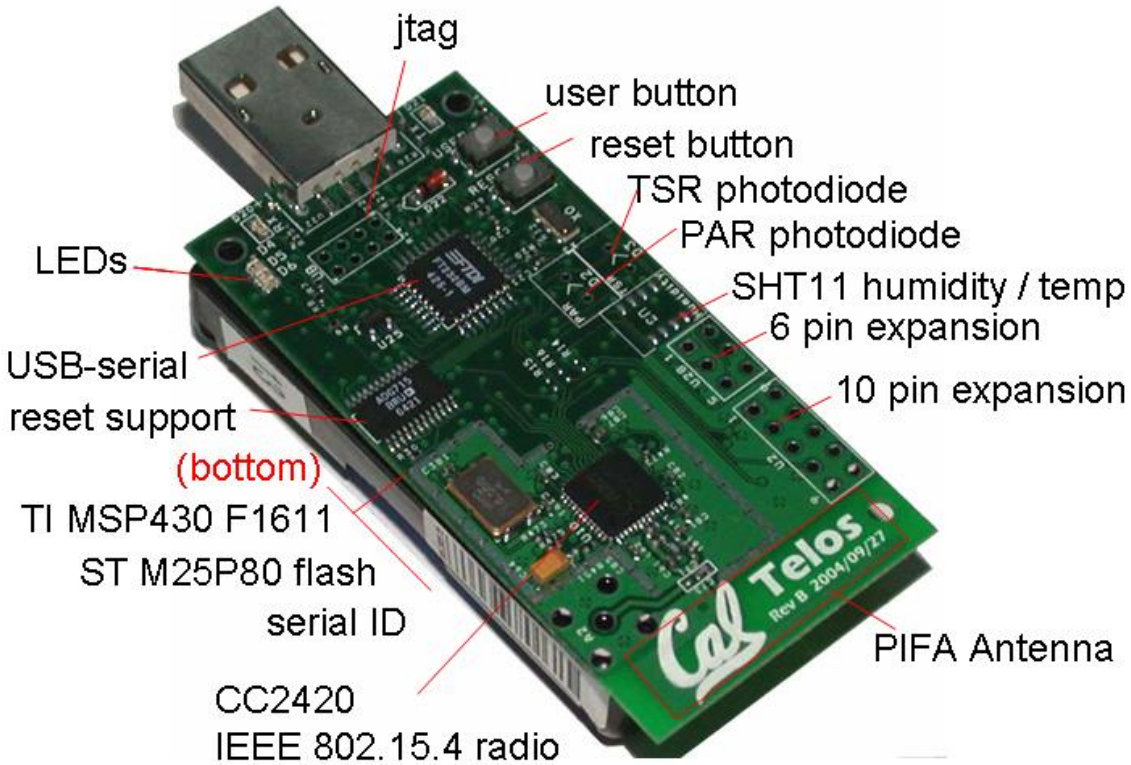

Figure 3.7: Telos-B mote similar to the one used in the experiments.

3.3 RSS measurements obtained from Telos-B motes

Telos-B motes are low power, open source, low cost motes developed by MEMSIC, Figure 3.7. They were developed to be a quick alternative for academic research and due to their relatively light weight, they are also used for inventory monitoring. A large (at least thirty-two by thirty-two feet) obstacle-free environment was needed in order to perform measurements, Kenney Hall was chosen as it provided the best environment. Telos-B mote experiments were performed in Kenney Hall, in building 642 at Wright-Patterson Air Force Base (WPAFB). Figure 3.8 shows the space where the Telos-B measurements were performed. The motes were placed on a stand approximately one meter above the floor to minimize ground interference and cardboard and plastic were used to construct the stands to minimize multi-path interference. Additionally, all motes were placed facing in approximately the same direction in order to minimize the effects of antenna orientation.

Figure 3.8: Location setup for motes used in experiments involving Telos-B and WARP/Wi-Pry hardware that were performed to obtain RSS measurements in Kenney Hall Auditorium at AFIT.

Twenty-five receivers in a 5×5 grid were placed on the stands throughout Kenney with eight feet between each mote. This left one mote to serve as a base station connected to the laptop, and six motes that could be moved to obtain the most measurements in the least amount of time. The experiment was started with number two, since the first experiment performed was used as a calibration and to verify motes were reporting properly.

Figure 3.9 shows the method used for obtaining measurements. The solid black boxes represent the twenty-five positions of the stationary receivers. The outlined boxes represent the position of six additional transmitter motes (labeled 26 – 31). These motes serve as transmitters for analysis purposes. All six transmitters were moved six times for 36 total

possible transmitter locations[1]. The data from the Telos-B is output as a 31×31 matrix which gives link RSS values from all motes to all other motes.

There is an eight foot spacing between motes except where mote placement falls in the center of a quadrant of motes, in which case there will be a four foot spacing. This happens between receiver motes $1 - 25$ and transmitter motes $26 - 31$. The outlined black box represents the initial starting position of the six receivers labeled $25 - 31$ and the gray outlined box represents the other five positions of receiver motes $25 - 31$ in experiment $3 - 7$. The first number in the box represent the experiment number (2-7) and the second number represents the receiver number. The red box around receiver thirteen indicates that this is the transmitter and the results from the T-test are based on this assumption. For example, $4 - 30$ is the location of mote thirty for experiment four.

3.3.1 T-Test for consistency of receiver RSS measurements across all experiments.

A data analysis similar to that performed on the SunSPOT data was performed for the Telos-B motes. Before the Telos-B measurements can be used to evaluate the proposed model and geolocation algorithms found in Chapters 4 and 5, some justification should be done as to the legitimacy of the measurements that were obtained. Past research with SunSPOT motes proved to be only 10% consistent, Figure 3.10, and most measurements obtained with these devices were unusable for geolocation purposes. It should be noted that since these measurements were performed in a metal rich environment, some error will exist in our results, but it is believed that the analysis in this section is justified. The error introduced into the RSS measurements is found in the range estimation part of Figure 1.1, specifically the effects from multi-path and shadowing will introduce some of the error seen in these RSS measurements.

[1]Note that even though motes $26 - 31$ are serving as transmitter locations, all motes can transmit and receive.

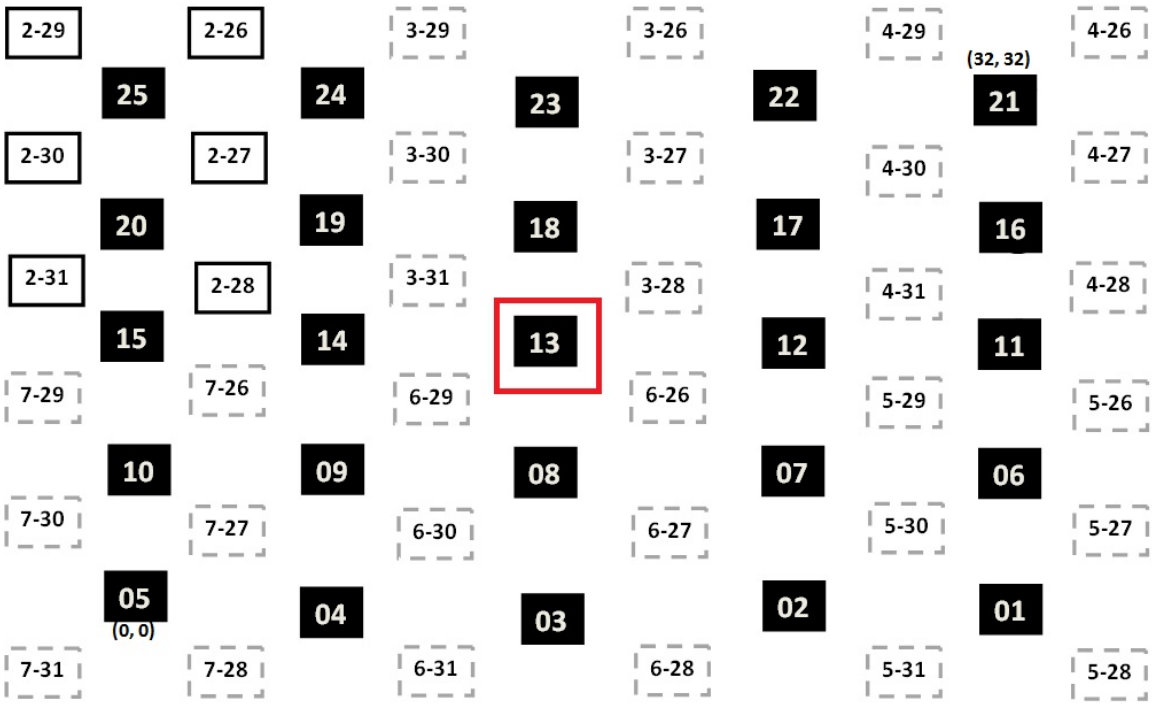

Figure 3.9: Graph showing locations of receivers for the measurements performed using Telos-B. Solid black boxes represent the location of the 25 stationary receivers, the outline black box represents the first six positions for receivers 26 – 31 and the grey dashed boxes are the other locations to where the six receivers were moved.

Table 3.4 on page 38 is a summary of the results of several T-tests that were run to compare the measurements obtained by the Telos-B in the six different measurement campaigns. The T-tests were used to check for consistency among the different experimental campaigns. Mote thirteen, which is located in the center of the 5×5 Telos-B grid, acts as the transmitter. Multiple T-tests were performed on the same data, therefore a Bonferroni correction to α is needed. Set $\alpha = 0.01$. In order to account for multiple tests, divide α by the number of T-tests being performed, fifteen, which gives an $\alpha = 0.01/15 = 0.00067$.

Our null and alternative hypothesis are, H_0 : RSS measurements are consistent across any two experiments vs. H_A : Not So. Reject the null hypothesis when $p < 0.00067$.

That would lead to a conclusion to reject the null hypothesis and conclude that there is a difference in the RSS measurements obtained from different experiments. A failure to reject the null hypothesis results in the conclusion that there is insufficient evidence to conclude that there is a difference in the mean measurements between experiments. Essentially a failure to reject the null ($p \geq 0.00067$) is desired, since it is desirable to have measurements that are consistent between experiments. All results should be interpreted in a similar fashion, column two in Table 3.4 is the percentage of consistent measurements across all experiments. For example, for mote 19, Telos-B measurements were consistent across all experiments 80% of the time.

Three motes had RSS measurements that were 100% consistent: nine, fourteen and twelve. This means that for mote nine, fourteen and twelve all of the p-values were above 0.00067 and there was a failure to reject of the hypotheses for these tests. It is encouraging that motes (12 and 14) on either side of the transmitter provide consistent RSS measurements 100%. Similar experiments performed using SunSPOT motes (in a less noisy environment than Kenney Hall) gave results that were inconsistent for similar receiver to transmitter distances. Figure 3.10 shows a pie chart comparing the percentage of consistent and inconsistent measurements for experiments performed using Telos-B motes (A) and SunSPOT (B) motes. With the SunSPOT motes there are less than 10% of consistent measurements, while over 50% of experiments performed with the Telos-B motes gave consistent measurements[2].

3.4 RSS measurements obtained from WARP board and Wi-Pry

This section focuses on measurements that were obtained from multiple transmitters. In order to easily obtain measurements from multiple transmitters, two WARP boards were used as transmitters and a Wi-Pry connected to an iPod was used as the receiver. Over

[2]Another benefit to the Telos-B is their ability to reset. If a bad packet is sent the Telos-B is able to resend the packet where as the SunSPOTs had to be manually restarted or simply reported *NaN*.

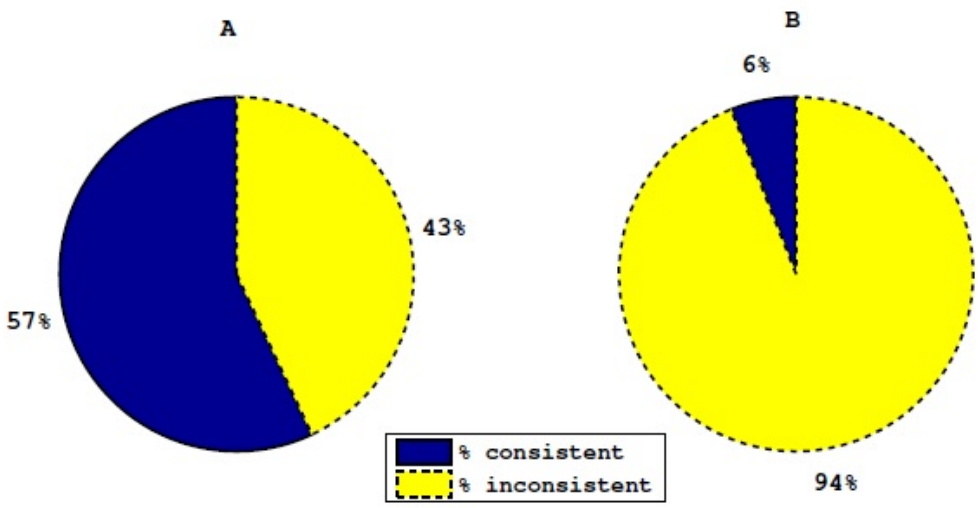

Figure 3.10: Percentage of consistent (blue solid) and inconsistent (yellow dash) measurements for Telos-B (A) and SUNSPOT (B) experiments.

a period of about two minutes, measurements were taken at each of the first twenty-five receivers shown in Figure 3.9. All testing conditions were the same as described in Section 3.4. Figure 3.12 shows one of the WARP boards that was used in the experiment.

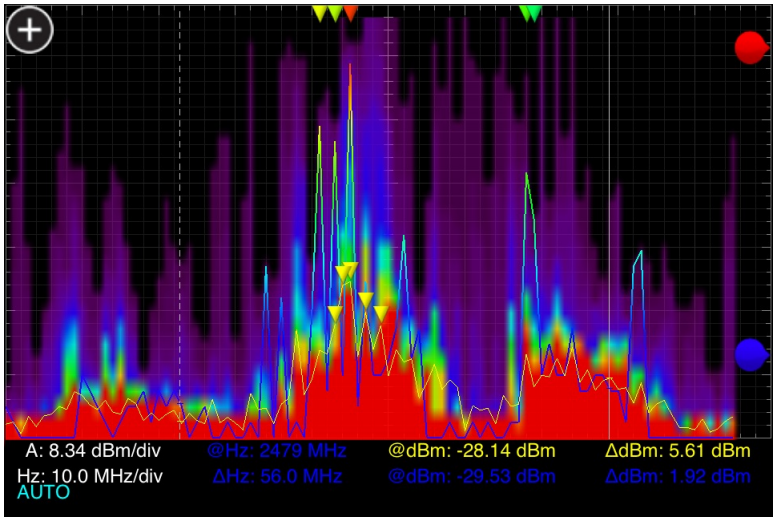

Figure 3.11: Screen shot of the Wi-Pry device used to measure RSS.

A Wi-Pry, Figure 3.11, is a low-cost power spectrum analyzer that operates in the 2.4 GHz band. While not specifically designed to demodulate the signal, it is possible to record the RSS coming from a transmitted signal. Since there are no other measurements to compare these measurements to, no analysis was done on the experiments, but the data was used in the validation process for multiple transmitters found in Chapters 4 and 5.

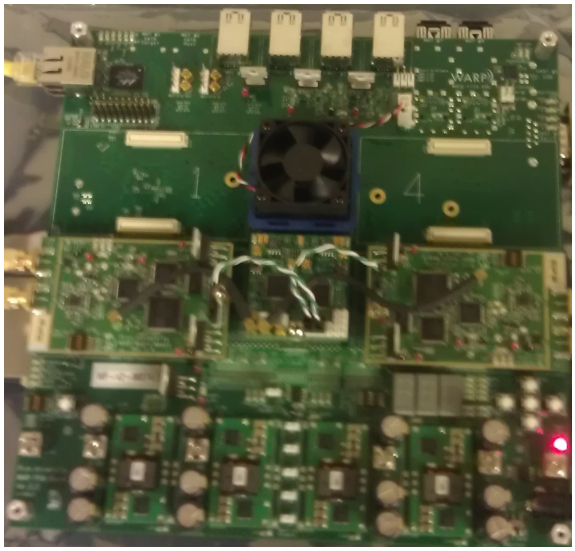

Figure 3.12: WARP board used for multiple transmitter experiments.

3.5 Conclusions about RSS experiments

This chapter examined performance of equipment that was used for validation purposes. It has been shown through statistical tests that the Telos-B motes perform more consistently even in an environment rich with multi-path. Due to this fact, their lower cost, ease of implementability and quickness in obtaining measurements, Telos-B measurements were chosen for validation of the algorithms proposed in Chapters 4 and 5. SunSPOTs were not used for validation of the algorithms as it was difficult to evaluate the RSS measurements for the experiments.

Table 3.4: Summary of T-tests comparing different experiments using Telos-B motes.

Receiver	**% of consistent measurements**
1	33%
2	47%
3	60%
4	53%
5	47%
6	87%
7	47%
8	27%
9	100%
10	40%
11	27%
12	100%
14	100%
15	60%
16	33%
17	27%
18	67%
19	80%
20	40%
21	53%
22	53%
23	53%
24	73%
25	73%

IV. Development of RSS Localization Methods

Several RSS models do not yield closed-form solutions for their estimated location, thus resulting in techniques that rely on approximations and iterations. Some authors assume that an RSS model fits a certain distribution. Along those lines many authors assume that since the sample sizes are generally so large, the distribution of RSS measurements is approximately Gaussian, which is a very liberal use of the Central Limit Theorem (CLT). The very popular Maximum Likelihood Equation (MLE) geolocation algorithm often produces multiple maximum values which results in multiple estimates of the transmitter position.

Based on (2.3), there are several algorithms available for location estimation [25]. Several of these procedures are derived in this chapter in addition to new algorithms derived during the course of this dissertation.

4.1 Derivation of a Maximum Likelihood Estimate

This algorithm, which is based on statistical theory, is straight forward to describe, but is not always easy to implement. It may be applied to any parametric family of distributions whose PDF is known. The MLE maximizes the probability of the transmitter location by minimizing the variance of estimated error. It performs well when the number of receivers is large, but may have more than one local maximum and often requires several iterations to converge. It also is strongly dependent on data coming from the chosen parametric family and when an incorrect family is chosen, it may not perform well. [3]

The MLE algorithm estimates the location of the transmitter using a log likelihood of the PDF, which describes the relationship between unknown variables and known variables. Let x denote a sample scalar value, with the Gaussian PDF, f then $f(p)$ is parameterized by its mean and variance.

[3] Maximizing the log-likelihood function is equivalent to minimizing the negative log-likelihood function.

$$f(\mathbf{p}, \mathbf{r}; \sigma^2) = \frac{1}{\sqrt{2\pi\sigma^2}} \exp\left(\frac{-\|\mathbf{p} - \mathbf{r}\|^2}{2\sigma^2}\right) \tag{4.1}$$

where $\mathbf{p}$ is the observed RSS values, $\mathbf{r}$ is the mean RSS value for sensor s and σ^2 is the amount of variance in the noise. Several different methods exist for solving (4.1). Taking the likelihood of (4.1) gives,

$$L = \prod_{s=1}^{S} \frac{1}{\sqrt{2\pi\sigma^2}} \exp\left(\frac{-\|\mathbf{p}_s - \mathbf{r}\|^2}{2\sigma^2}\right). \tag{4.2}$$

Since log is an increasing function it is much simpler to minimize the log of (4.2) to get

$$\begin{aligned} \mathcal{L} &= \log\left(\textstyle\prod_{s=1}^{S} \frac{1}{\sqrt{2\pi\sigma^2}} \exp\left(\frac{-\|\mathbf{p}_s - \mathbf{r}\|^2}{2\sigma^2}\right)\right) \\ &= \frac{1}{(\sqrt{2\pi\sigma^2})^S} \exp\left(\frac{\sum_{s=1}^{S} -\|\mathbf{p}_s - \mathbf{r}\|^2}{2\sigma^2}\right) \\ &= \ln(1) - S \ln \sqrt{2\pi\sigma^2} - \left(\frac{\sum_{s=1}^{S} -\|\mathbf{p}_s - \mathbf{r}\|^2}{2\sigma^2}\right), \end{aligned} \tag{4.3}$$

where p_s is the received signal strength, r is RSS data and σ^2 is the noise in the signal. Ignoring constants that do not affect the minimization gives,

$$\hat{z} = \arg\min_{z_0}\left(\sum_{s=1}^{S} \|\mathbf{p}_s - \mathbf{r}\|^2\right) \tag{4.4}$$

where $\mathbf{p}_s$ is the observed power, $\hat{z}$ is related to $\mathbf{p}_s$ through (2.3) since there is an inversely proportional relationship between distance and RSS and z_0 is a component in the distance calculation for d_s and $\mathbf{r}$ is the noise free RSS data. Equation (4.4) is the argument that minimizes the sum of squared error.

When the estimates of the MLE are extremely complicated nonlinear functions or involve a large number of parameters, a closed-form solution may not be readily available. Thus, iterative procedures must be employed, some of which are described in the next section.

4.1.1 Transmitter localization using MLE-GRID.

Since all receiver locations are known, a search space which contains a set of the known locations may be formed for the algorithm to search along. This is a fairly simple

process but may be computationally intensive to use for large, dense grid spaces. The algorithm computes the log likelihood for each search point, then chooses the search point that yields the maximum value. A grid-based MLE algorithm finds the minimum or maximum value of the likelihood function by searching a grid containing all possible locations for the sensor. For large search areas this algorithm takes an exorbitant amount of time and must search in both the x and y directions.

4.1.2 Transmitter localization using MLE-EM.

The Expectation Maximization (EM) algorithm alternates between performing an expectation step (E), which computes the expectation of the log-likelihood evaluated using the current estimate of the parameters and the maximization (M) step which computes parameters maximizing the expected log-likelihood found in the E step. The procedure repeats this process until the difference between estimates is sufficiently small or a set number of iterations have been performed. The solution generally depends on good initialization values which must be obtained a priori and may take several iterations before convergence to a single local maxima occurs.

4.1.3 Transmitter Localization using MLE-GD.

The gradient descent algorithm is based on the observation that the likelihood function decreases fastest when it goes from its initial estimate in the direction of the negative gradient. A gradient descent method is a first order optimization algorithm in which to find the argument that maximizes the log-likelihood of a function. Define a step size, $\gamma > 0$, an initial starting position $[x_0, y_0]$, then the new positions $\hat{x}_0$ and $\hat{y}_0$ in the descent are given by:

$$\begin{aligned} \hat{x}_0 &= x_0 - \gamma \frac{\partial \mathcal{L}}{\partial x} x_0 \\ \hat{y}_0 &= y_0 - \gamma \frac{\partial \mathcal{L}}{\partial y} y_0 \end{aligned} \tag{4.5}$$

where $\frac{\partial \mathcal{L}}{\partial x}, \frac{\partial \mathcal{L}}{\partial y}$ are the partial derivatives of the likelihood function with respect to x and y.

Algorithm 1 :MLE-EM

procedure Q-EM(a, b) ▷ a is lower bound b is upper bound
  Initial random value $z_m^{(0)} \sim UNIF(a, b)$
  Find the Expected value of the Log-likelihood using $z_m^{(0)}$
  $\mathbf{p}^{(t)} = E(\mathbf{p}|z_m^{(0)})$
  Maximize Log-likelihood to find new estimate
  $z_m^{(t)} = \arg\max_{(x_0,y_0)}(\log(f(\mathbf{p}^{(t)}|z_m^{(0)})))$
  while $z_m^{(t)} - z_m^{(t-1)} \geq \tau$ **do** ▷ τ is the tolerance level for stopping the algorithm
    Step 2
    Step 3
    Step 4
  end while
  return $\hat{z}_m$ ▷ The final location estimate is $\hat{z}$
end procedure

Algorithm 2 :MLE-GD

procedure GD(a, b) ▷ a is lower bound b is upper bound
  $x_{old} = 0$
  Initial random value $x_{new} \sim UNIF(a, b)$
  Define γ ▷ Step size value.
  Define τ ▷ Tolerance level.
  while $|x_{new} - x_{old}| > \tau$: **do**
    $x_{old} = x_{new}$
    $x_{new} = x_{old} - \gamma * f_{prime}(x_{old})$
  end while
  return $\hat{z}_m$ ▷ The final location estimate is $\hat{z}_m$
end procedure

4.2 Transmitter localization using MLE for a correlated noise fading RSS

The development of an MLE which considers correlated noise fading differs slightly than that for independent fading by using a covariance matrix to account for the correlation between the noise terms.

4.2.1 Literature review of algorithms using correlated fading RSS.

Flam et al. [11] perform a geometrically complex algorithm which requires 100 different initial positions, and thus would be much more time consuming than the algorithm that this research proposes. They showed that better accuracy is achieved with a Weighted Least Squares (WLS) estimation method than with Weighted Average (WA) estimation. Their explanation of MLE does not use a log-likelihood but rather they find the argument that maximizes the PDF. In order to locate the source, they use an approach which relies on the assumption of a posterior distribution. As a result, they rely on a localization algorithm that floods the search space with possible transmitter locations. They showed that they could achieve better accuracy with a WLS estimation method than with Weighted Average (WA) estimation.

Al-Dhalaan and Lambadaris [12] relax the PDF of the mean RSS in order to directly find the estimated location. A special software solver is used to find the location, due to the mathematical complexity of the problem.

4.2.2 Development of MLE for correlated noise fading RSS.

This research introduces the use of correlated noise fading measurements, $\mathbf{w} \sim N(\mathbf{0}, \mathbf{\Sigma})$, in the derivation of the RSS model. If the covariance matrix, Σ is defined as $\sigma^2 > 0$ along the diagonal and $\rho\sigma^2$ on the off-diagonal matrix, then Σ is expressed as a measure of the amount of correlation in the noise term,

$$\mathbf{\Sigma} = \sigma^2 \left(\rho \mathbf{1}_S \mathbf{1}_S{}^T + (1-\rho)\mathbf{I}_S \right) . \tag{4.6}$$

Note that all ρ are the same for simplicity, but could be varied to fit other models. Consider the normal PDF.

$$f(\mathbf{p};\mathbf{r},\mathbf{\Sigma}) = \frac{1}{\sqrt{2\pi}|\mathbf{\Sigma}|^{1/2}} \exp\left[-(\mathbf{p}-\mathbf{r})^T\mathbf{\Sigma}^{-1}(\mathbf{p}-\mathbf{r})\right] \tag{4.7}$$

where $\mathbf{p}$ is the observed RSS values, $\mathbf{r}$ is the mean RSS value defined in (2.1) and $\mathbf{\Sigma}$ is the covariance matrix of the noise. Expressed in matrix terms as,

$$L = \prod_{s=1}^{S} \frac{1}{\sqrt{2\pi}|\mathbf{\Sigma}|^{1/2}} \exp\left[-(\mathbf{p}-\mathbf{r})^T\mathbf{\Sigma}^{-1}(\mathbf{p}-\mathbf{r})\right]. \tag{4.8}$$

The next step involves taking the likelihood of the (4.7). It is much simpler to maximize the log of (4.8):

$$\begin{aligned} \mathcal{L} &= \ln\left(\tfrac{1}{(\sqrt{2\pi}(|\mathbf{\Sigma}|^{1/2}))^S} \exp\left[-(\mathbf{p}-\mathbf{r})^T\mathbf{\Sigma}^{-1}(\mathbf{p}-\mathbf{r})\right]\right) \\ &= -S\ln\left(\sqrt{2\pi}|\mathbf{\Sigma}|^{-1/2}\right) - \left((\mathbf{p}-\mathbf{r})^T\mathbf{\Sigma}^{-1}(\mathbf{p}-\mathbf{r})\right). \end{aligned} \tag{4.9}$$

Ignoring constants that do not affect the minimization gives

$$\hat{z} = \arg\min_{z_0}\left((\mathbf{p}-\mathbf{r})^T\mathbf{\Sigma}^{-1}(\mathbf{p}-\mathbf{r})\right), \tag{4.10}$$

where $\mathbf{\Sigma}^{-1}$ is the inverse of the correlated noise fading. The equation in (4.10) is true for any model of $\mathbf{\Sigma}$. For $\mathbf{\Sigma} = \sigma^2\mathbf{I}$ which implies that $\mathbf{\Sigma}^{-1} = \frac{1}{\sigma^2\mathbf{I}}$ it can be simplified as,

$$\begin{aligned} \hat{z} &= \arg\min_{z_0} \tfrac{1}{\sigma^2}\left[\mathbf{p}^T\mathbf{p} - \mathbf{p}^T\mathbf{r} - \mathbf{r}^T\mathbf{p} + \mathbf{r}^T\mathbf{r}\right] \\ &= \arg\min_{z_0} \frac{\left(\mathbf{p}^T\mathbf{p} - 2\mathbf{p}\mathbf{r} + \mathbf{r}^T\mathbf{r}\right)}{\sigma^2} \\ &= \arg\min_{z_0} \frac{(\mathbf{p}-\mathbf{r})^2}{\sigma^2} \\ &= \arg\min_{z_0} \|\mathbf{p}-\mathbf{r}\|_2 \end{aligned} \tag{4.11}$$

where $\|\cdot\|_2$ is the two norm. This algorithm was validated using measurements obtained from the Telos-B measurement campaign.

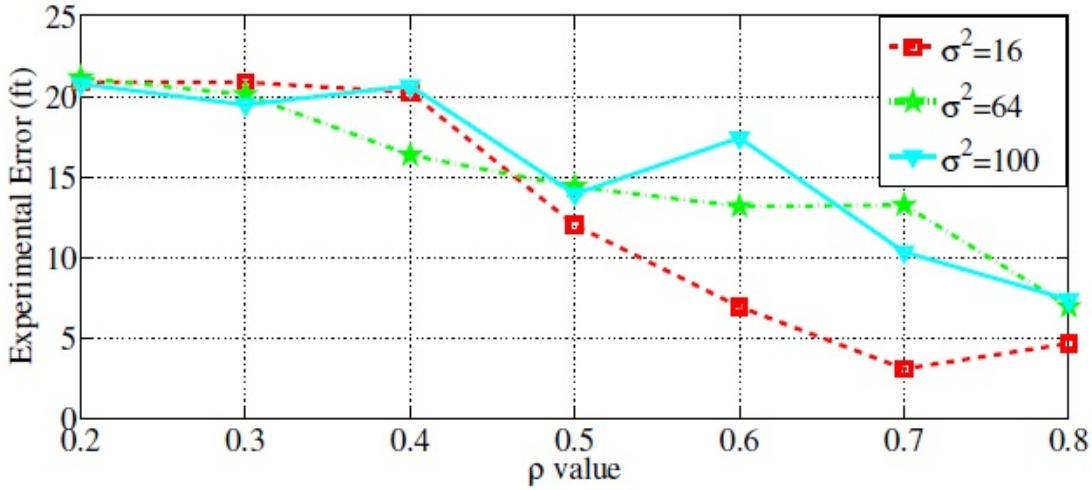

Figure 4.1: RMSE versus correlation for the estimated transmitter location assuming a correlated fading model and using measurements obtained from experiment six in Chapter 3. The squares correspond to $\sigma^2 = 16$, the stars correspond to $\sigma^2 = 64$ and the triangles correspond to $\sigma^2 = 100$.

4.2.3 Experimental validation of correlated fading model and algorithm.

The six experimental RSS measurements were plotted against the distances in dB and a line was fit in order to find estimates for P_0 and η. Therefore, $P_0 = 43$ dBm and $\eta = 1$ were chosen for the validation purposes.

Figure 4.1 shows the RMSE for the estimated transmitter location assuming a correlated fading model and using data obtained from the Telos-Bs. There are three different variances shown and it would appear that a variance of $\sigma^2 = 16$ gives the most accurate estimate of the transmitter location. For a $\rho = 0.8$ the experimental error of the transmitter location is 4.669 feet, when $\rho = 0.5$ the experimental error is 12.01 feet. Conclude that when measurements are highly correlated, ($\rho = 0.8$) the location of the transmitter which is actually located at (16, 16) can be estimated to within 5 feet.

4.3 Development of MLE for multiple antenna RSS

In this section all RSS measurements are assumed to be from a Gaussian Mixture Model (GMM) distribution. Three different MLE algorithms were explored: (1) the MLE derived for the widely accepted standard path-loss log-distance model (herein known as MLE-STND) (2.3), (2) the MLE derived for a GMM (MLE-GMM), and (3) the standard MLE derived using the gain between the antennas averaged out (MLE-STND-A). STND-A explores whether a standard MLE algorithm could be used if the average gain from the two antennas was subtracted out in the algorithm. The MLE of the location is the argument that minimizes the log-likelihood of (4.7). The likelihood and log-likelihood functions are found below. Since the transmitter has multiple antennas, the signal may come from either antenna with equal probability. Thus, RSS measurements may be modeled by a GMM of the measurements coming from all N antennas. The probability of RSS, $\mathbf{r}$, in the mixture of N Gaussian components is given by,

$$f(\mathbf{p};\mathbf{r}) = \sum_{n=1}^{N} \varpi_n f(\mathbf{p};\mathbf{r}_n) \tag{4.12}$$

$$= \sum_{n=1}^{N} \frac{\varpi_n}{\sqrt{2\pi}\sigma_n} \exp\left(\frac{-\|\mathbf{p}-\mathbf{r}_n\|^2}{2\sigma^2{}_{sn}}\right) \tag{4.13}$$

where ϖ_n is the weight associated with the n^{th} antenna. Given a RSS measurement, the probability of the signal coming from the mixture of S Gaussian sensors is modeled as (2.13). The first step in the algorithm is to find the likelihood of (4.12)

$$L = \prod_{s=1}^{S} \sum_{n=1}^{N} \frac{\varpi_n}{\sqrt{2\pi}\sigma_{sn}} \exp\left(\frac{-\|\mathbf{p}_s-\mathbf{r}_{sn}\|^2}{2\sigma^2{}_{sn}}\right), \tag{4.14}$$

Again, it is more convenient to maximize the log likelihood than the likelihood. Therefore, taking the natural log of (4.14) gives,

$$\mathcal{L} = \ln\left(\prod_{s=1}^{S} \sum_{n=1}^{N} \frac{\varpi_n}{\sqrt{2\pi}\sigma_{sn}} \exp\left(\frac{-\|\mathbf{p}_s-\mathbf{r}_{sn}\|^2}{2\sigma^2{}_{sn}}\right)\right) \tag{4.15}$$

$$= \sum_{s=1}^{S} \ln\left\{\sum_{n=1}^{N} \frac{\varpi_n}{\sqrt{2\pi}\sigma_{sn}} \exp\left(\frac{-\|\mathbf{p}_s-\mathbf{r}_{sn}\|^2}{2\sigma^2{}_{sn}}\right)\right\}. \tag{4.16}$$

This equation cannot be simplified any further by hand, since no closed-form solution exists. The maximum likelihood function (MLE-GMM) is the function that maximizes the log likelihood (4.14), given by

$$\hat{z} = \arg\max_{(x_0,y_0)} \sum_{s=1}^{S} \ln \left\{ \sum_{n=1}^{N} \frac{\varpi_n}{\sqrt{2\pi}\sigma_{sn}} \exp\left[-\frac{(p_s - r_{sn})^2}{2\sigma_{sn}^2} \right] \right\} \tag{4.17}$$

where ϖ_n is the weight of the n^{th} antenna.

4.3.1 Simulations for multiple antenna RSS model and algorithm.

MATLAB was used to simulate an environment with sixty-four receivers in a uniform square pattern. The first scenario investigated used concentric boxes spaced around a transmitter located at the origin. All receivers and boxes are assumed to be spaced equally.

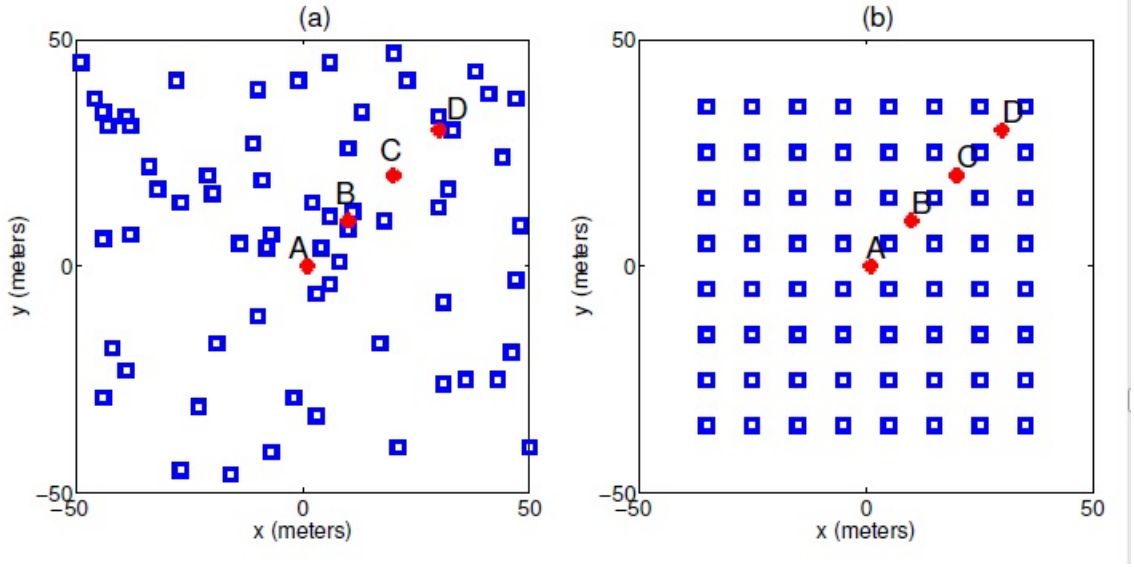

Figure 4.2: Receiver placement geometry used to perform simulations, asterisks represent the true transmitter location and squares represent the receiver positions. Positions A, B, C, D will be used in the remainder of this section to denote the different transmitter positions for the corresponding experiments. Figure (a) shows random receiver placement and (b) is square receiver placement.

Figure 4.2 shows the placement of the sixty-four receivers that were used in the simulations in this section, with the transmitter located in the center at $(0, 0)$. To minimize results biased from small sample size, one thousand trials were run for each set of boxes. Two different realistic scenarios were examined, (i) square placement of the receivers and (ii) random placement of receivers. Both cases were simulated using 64 receivers.

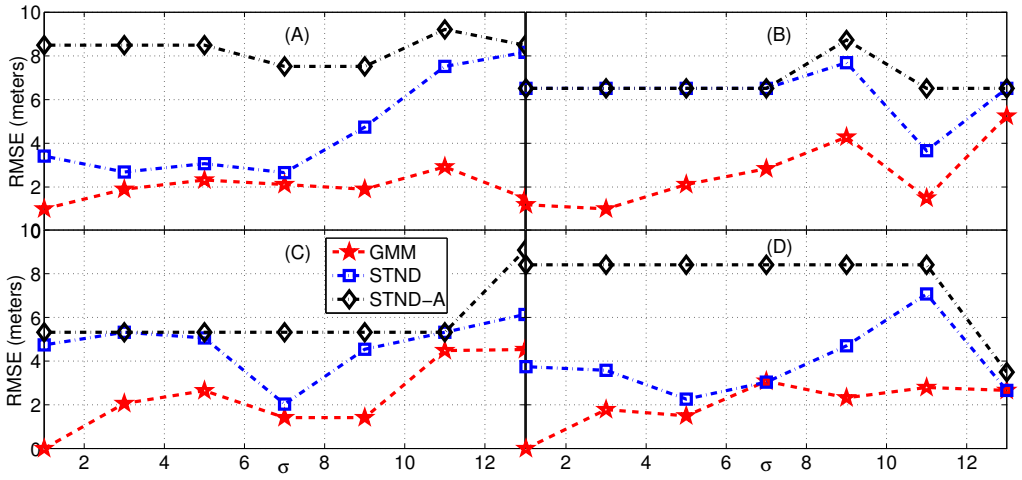

Figure 4.3: RMSE versus σ for estimated transmitter location when true receiver is located as in Figure 4.2 for random receiver placement after 5000 trials. Figure (A) is the transmitter located at $(0, 0)$, (B) is transmitter at $(10, 10)$, (C) is transmitter at $(20, 20)$ and (D) is the transmitter located at $(30, 30)$.

Figure 4.3 shows the RMSE values for our three scenarios described above for a random placement of sensors. For the case where the transmitter is located at (B), the two standard algorithms perform similarly. This may be due to the fact that the transmitter located in (B) is actually placed on top of three receivers. For the other three graphs (A, C, D), as the amount of fading increases, RMSE of MLE-STND remains relatively constant with a few peaks. This is not altogether unexpected since MLE-STND and MLE-STND-A are not appropriate estimation techniques for RSS-GMM data. It is not appropriate to use a

MLE-STND or MLE-STND-A algorithm for estimating location when RSS measurements are from a GMM distribution. This would result in a much larger error in the location accuracy than if the MLE-GMM algorithm was used.

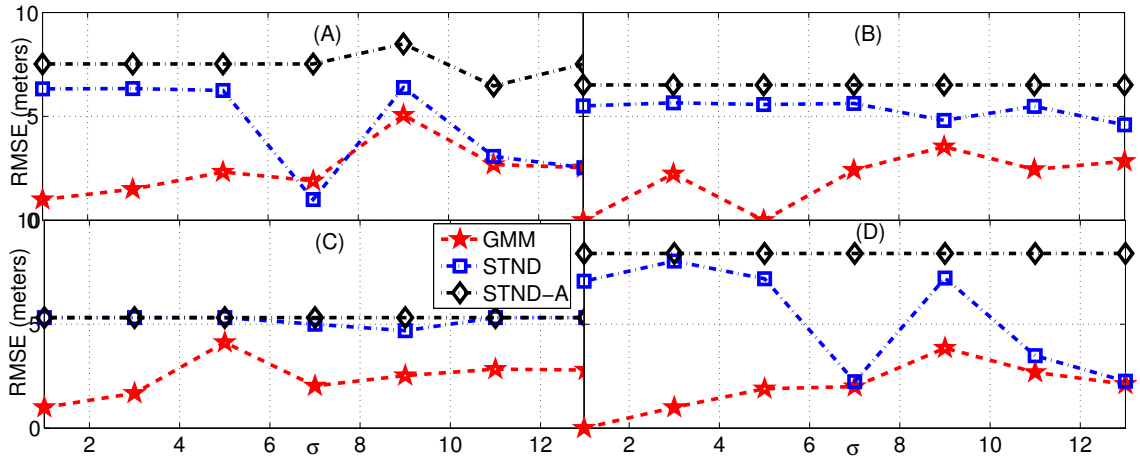

Figure 4.4: RMSE vs. σ for estimated transmitter location when true receiver is located as in Figure 4.2 for square receiver placement after 5000 trials. Figure (A) is the transmitter located at $(0, 0)$, (B) is transmitter at $(10, 10)$, (C) is transmitter at $(20, 20)$ and (D) is the transmitter located at $(30, 30)$.

Figure 4.4 shows RMSE values for a square placement of sensors. If the RSS coming from the antennas is actually from a GMM distribution but is located using a MLE-STD or STD-A, the location error would be greater than if the data had been modeled using a MLE-GMM. The MLE-GMM algorithm performs better than either of the standard algorithms. That is to be expected since technically both standard algorithms are a "wrong" fit for the RSS-GMM data. To reiterate, when the MLE-STND or MLE-STND-A algorithms are used and the data is RSS-GMM, even when fading is small ($\sigma = 1$), the RMSE is still very large (as much as eight meters).

4.3.2 Performance analysis of proposed GMM model and algorithm.

It is important to examine the performance of the MLE under different conditions. This is done by looking at the RMSE versus the numbers of receivers for varying path-loss values. It is expected that as the number of receivers increases the RMSE should decrease.

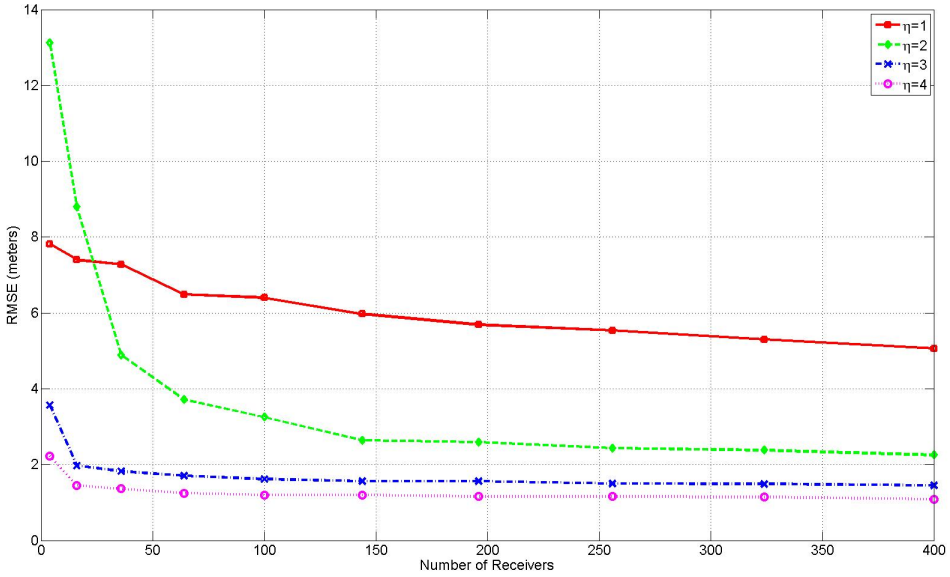

Figure 4.5: RMSE versus number of receivers for varying values of η.

As shown in Figure 4.5, when the GMM is considered over the single Gaussian as a way to model the RSS and locate the transmitter, it always performs better for the square receiver placement. It appears that as the environment becomes more cluttered, which increases path-loss, the location error actually drops. As is expected for both of these scenarios, at all path-loss values, RMSE decreases as the number of receivers increases. This is not the case for the random placement scheme, as mentioned before.

When antenna diversity is taken into account, it is generally a good idea to use a RSS-GMM model and a MLE-GMM algorithm. Additional research could involve investigating why the random placement scheme does not perform as well as the other scheme. Also, a

cost function may need to be developed to increases the accuracy of the transmitter location estimate. This might suggest that it is more appropriate to use the RSS-GMM in situations when large path-loss values are expected. Experimental validation of the RSS-GMM model for dual antennas could also be investigated.

4.4 MLE derivation for RSS-COOP and RSS-NC models and simulations

This author derived the MLE for the non-cooperative and cooperative RSS models discussed in Chapter 2. This section derives a novel Maximum Likelihood Estimate Cooperative (MLE-COOP) and Maximum Likelihood Estimation Non-Cooperative (MLE-NC) algorithm for use with these models and provides simulations for locating transmitters using these algorithms. Knowing that $\mathbf{p}_{coop}$ follows a Normal distribution allows expression of the PDF as,

$$f(\mathbf{p}_{coop}; \mathbf{r}) = \frac{1}{\sqrt{2\pi\sigma^2}} \exp\left[-\frac{\|\mathbf{p}_{coop} - \mathbf{r})\|^2}{2\sigma^2}\right]. \tag{4.18}$$

Following the steps described in this chapter a MLE was derived from (4.18),

$$\mathcal{L} = \arg\min_{z_0} \left((\mathbf{p}_{coop} - \mathbf{r})^T (\mathbf{p}_{coop} - \mathbf{r})\right). \tag{4.19}$$

Similarly the log-likelihood of the non-cooperative model may be found via,

$$\mathcal{L} = \arg\min_{z_0} \left((\mathbf{p}_{nc} - \mathbf{r})^T (\mathbf{p}_{nc} - \mathbf{r})\right). \tag{4.20}$$

Expressions in (4.19) and (4.20) could be solved using a grid search, EM or gradient descent. Here a grid search method was used and $\mathbf{r}$ depends on z_0 via (2.12) and (2.3).

4.4.1 Simulations for cooperative and non-cooperative RSS models.

Simulations, Figures 4.6 and 4.7 on page 52 and page 53 respectively, showed that Root Mean Squared Error (RMSE) was lower for non-cooperative. By assuming that sensors are cooperative when they are actually non-cooperative, a conclusion is made that the transmitters are closer than they actually are. This provides a false sense of accuracy of the transmitter locations and therefore it is important to consider whether transmitters

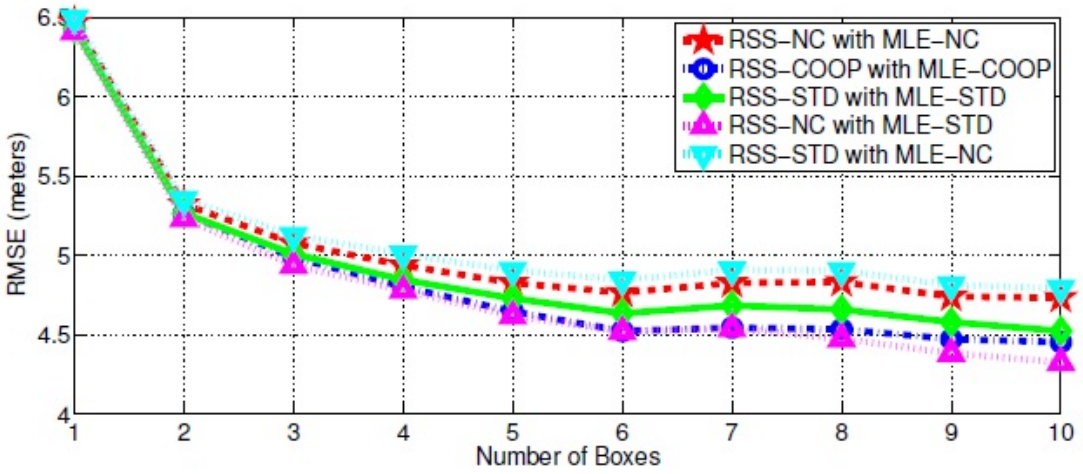

Figure 4.6: RMSE versus number of boxes for non-cooperative, cooperative, standard log-normal models (correct fits) and the non-cooperative with a MLE-STD, standard with MLE-NC (wrong fits).

are cooperative or non-cooperative when deciding which algorithm to use to locate them. When signals are cooperative it is important to consider the noise floor that is present in the estimates and truncate the signals accordingly. Doing this for cooperative signals will lead to more accurate estimates of the transmitter location (MLE-COOP) than by including noise floor measurements in the calculation of the transmitter location (MLE-STD).

4.5 MLE derivation of multiple transmitter RSS model

The field of multiple transmitter localization is largely dominated by Nelson et al. [26], [21], [27], [28]. Much of their research involves a quasi-EM algorithm and forms the basis for this author's results found in Chapters 4-5. To perform quasi-EM localization the following steps should be performed:

Step 1 Generate random initial starting positions for each of the M transmitters from a uniform distribution, $\hat{z}_m \sim UNIF(-100, 100)$.

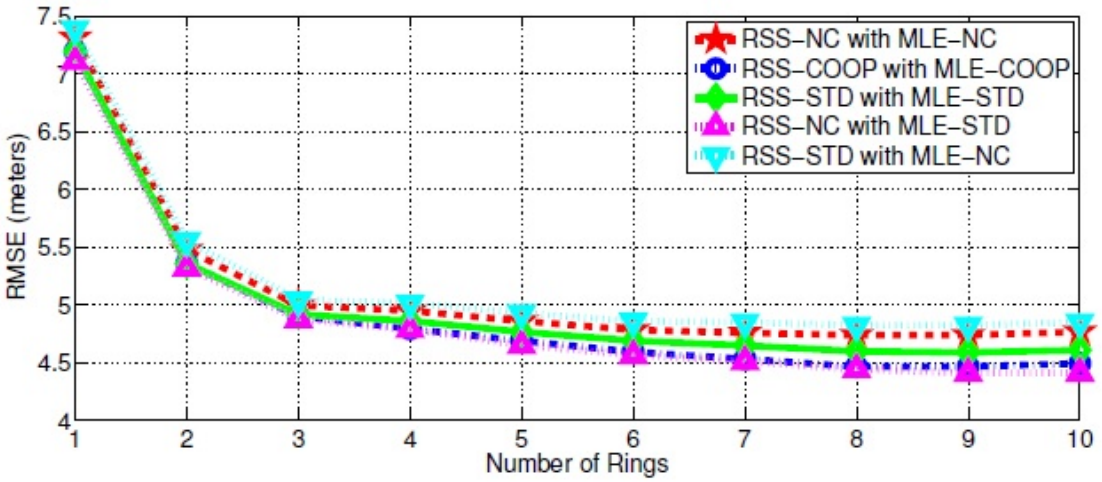

Figure 4.7: RMSE versus number of circles for non-cooperative, cooperative, standard log-normal models (correct fits) and the non-cooperative with a MLE-STD, standard with MLE-NC (wrong fits).

Step 2 Compute the expected RSS power at the s^{th} receiver from the m^{th} transmitter.

$$E_{ms} = \left(\frac{P_0 d_0^{\eta}}{d_s(\hat{z}_m)^{\eta}} \right) \tag{4.21}$$

where P_0 is the transmit power, d_0 is the close-in reference distance generally taken to be one, $d_s(\hat{z}_m)$ is the distance from the estimated location of the m^{th} transmitter to the s^{th} receiver.

Step 3 Normalize the values found in step two so that they give a total power at each receiver that is equal to the observed power at that receiver, converted to dB,

$$\tilde{E}_{ms} = \frac{P_s E_{ms}}{\sum_{K=1}^{M} E_{Ks}} \tag{4.22}$$

$$\tilde{e}_{ms} = 10 \log_{10}(\tilde{E}_{ms}). \tag{4.23}$$

Step 4 For each transmitter M, solve:

$$\hat{z}_m = \arg \min_{z_m} \sum_{s=1}^{S} \left(\tilde{e}_{sm} - 10 \log_{10} \left(\frac{P_0 d_0^{\eta}}{d_s(\tilde{z}_m)^{\eta}} \right) \right)^2 \tag{4.24}$$

where $\tilde{e}_{sm}$ is the normalized power at each receiver, $d_s(\tilde{z}_m)$ is the distance from each receiver to the estimate of transmitter location, P_0 is the constant transmit power, d_0 is the close in reference distance and η is the path-loss exponent. The algorithm repeats steps two through four using $\hat{z}_m$ for a set number of iterations that is sufficient for convergence. The number of initializations corresponds to the number of times step one is run and a cost function is necessary to find the sum-squared difference in received and estimated log power. A cost function is necessary because the MLE may not always have one global minimum value.

Step 5 Looking at the final estimates obtained at each initialization, a cost function was developed to decide on the best estimate. The cost function is defined to be

$$C = \sum_{s=1}^{S} \left(\log_{10}(R_s) - \log_{10} \sum_{m=1}^{M} \left(\frac{P_0 d_0^{\eta}}{d_s(\hat{z}_m)^{\eta}} \right) \right)^2 \tag{4.25}$$

where R_s is the power in linear terms, $d_s(\hat{z}_m)$ is the distance from the final estimate of transmitter location for each random initialization and η is the path-loss exponent.

Equations (4.24)-(4.25) are repeated until the value of C is acceptable. This repetition implements a quasi-EM algorithm.

4.5.1 Simulations for MLE and model of multiple transmitters.

The following parameters were assumed for this simulation: $P_0 = 20$ dB, $\eta = 2$, $d_0 = 1$ meter and $\sigma^2 = 16$. Also assume that the location of receivers is known. Only the case of 100 receivers with noise variance of sixteen is shown here, since, this is not a novel algorithm and these results were mainly used for comparison with DRSS-M results.

Figure 4.8 shows the actual (x_m, y_m) and path that is taken by each initialization to get to the estimated $(\hat{x}_m, \hat{y}_m)$ using the MLE function for the case of 100 receivers and two transmitters with a noise variance of sixteen for four random initializations. True transmitter location is indicated by a **x** and final estimated transmitter position is contained in the circle. The first initialization is represented by a dot, the second initialization

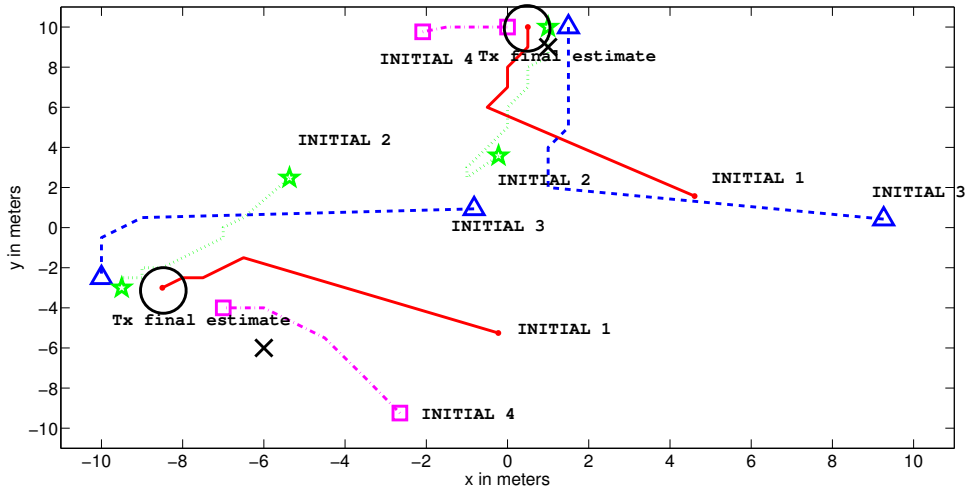

Figure 4.8: Actual (x_m, y_m) and path that is taken by each initialization to get to the estimated $(\hat{x}_m, \hat{y}_m)$ using the MLE function. True transmitter location is indicated by a **x** and final estimated transmitter position is contained in the circle. The first initialization is represented by a dot, the second initialization is represented by a star, initialization three is represented by a triangle and the fourth initialization is represented by a square.

is represented by a star, initialization three is represented by a triangle and the fourth initialization is represented by a square. Each axis is in meters. Figure 4.8 shows that all initializations appear to be converging to a reasonable estimate which suggests that the algorithm is performing well.

V. Development of DRSS Model and Algorithms

Geolocation using RSS is a popular technique because no additional hardware is required and measurements are computationally inexpensive. However, this type of localization is not without its drawbacks. One major drawback is the assumption of constant transmit power. This assumption may be alleviated by using DRSS measurements. While literature exists on DRSS measurements, most assume uncorrelated RSS (and DRSS measurements) and suffer from computationally complex algorithms or oversimplification of the system by linearizing measurements.

This chapter addresses these shortcomings by exploring the use of DRSS measurements for geolocation under a spatially correlated shadowing model. To the author's knowledge, a correlated noise model for RSS measurements that results in correlated noise in the DRSS measurements has been investigated before but not with the associated MLE. This dissertation also proposes a novel gradient descent approach to compute the MLE, leading to accurate geolocation under reduced computational complexity. This section discusses previous models but does not provide the differences in our model and the established models.

5.1 Literature review of current DRSS localization methods

This chapter begins with a review of existing literature on independent and correlated DRSS measurements and their corresponding localization algorithms.

Assad et al. [14] utilize RFID technology for their real time experiment. Even though this is not directly applicable to our research, they do incorporate a correlated log normal shadowing term and then use positioning software to solve the model. Some of their assumptions differ from the assumptions in this dissertation. They do not assume a constant

variance, thus increasing the complexity of the problem. They assume an exceptionally high correlation coefficient ($\rho = 0.96$).

Stationary Signal Strength Difference (SSSD) is explored extensively by Liu et al. [29–31], its application is in cellular networks but due to the limited literature on DRSS it is considered here. They use a SSS-D model which includes an auto-correlation function to account for correlated fading and considers the antenna height. Intersection equations are found and then a least squares procedure is used to locate the transmitter. Liu et al. [29–31] linearize the power measurements, include an extra variable in antenna height, do not assume a constant transmit power and express η as a function of antenna height. Their localization technique is considerable more complex and they use a least squares procedure.

Wang et al. [32–35] use a noise model which does not account for correlation. They generally use a least squares procedure to locate the transmitter.

Jackson et al. [32–35] investigate DRSS in depth. Much of their research assumes RSS and DRSS measurements are independent and uncorrelated. A recent paper by Jackson et al. proposes a correlated DRSS matrix where the correlated fading term is the sum of two correlated noise terms but does not consider a correlation coefficient. A least squares solution is found.

Lee and Buehrer [15] provide similar research into correlated RSS and DRSS measurements and then use a least squares approach which utilizes redundant differences. They do not make direct use of the MLE and therefore all of their proposed methods are more computationally complex and require a greater number of operations. Lee et al. [15] use a geometric interpretation to localize the sensor and consider redundant measurements while this research considers only unique measurements. Their use of Least Squares estimations also means that all of their equations must be linearized before estimation can begin. Also the use of redundant measurements to improve RMSE may be time consuming.

Mailaender et al. [36] use correlated RSS and DRSS measurements, however they compute the theoretical Cramer Rao Lower Bound (CRLB) and do not specifically locate the transmitter.

5.2 Derivation of a DRSS model

The model used in this chapter assumes that RSS measurements are correlated and may be described by a correlated fading model. All vectors are column vectors unless noted otherwise, and $(\cdot)^T$ denotes transpose. In its simplest form (assuming independent measurements), DRSS involves subtracting the $S-1$ pairs of RSS measurements. For simplicity, define a reference receiver $s = 1$ and subtract all $s > 1$ terms from that. Define a matrix A to constrain the measurements so that there are $S-1$ unique measurements. Let $\mathbf{p} = [p, ..., p_S]^T$. Define matrix $\mathbf{A}$ and vector $\mathbf{p}$ such that $\mathbf{Ap}$ is the matrix that contains all $S-1$ combinations,

$$\mathbf{A} = [\mathbf{1}_{(S-1)\times 1}, -\mathbf{I}_{(S-1)\times(S-1)}] \; . \tag{5.1}$$

Form $S-1$ DRSS combinations, q, by multiplying (5.1) by (2.3)

$$\mathbf{q} = \mathbf{Ap} = 10\eta \log_{10}\left(\frac{\mathbf{d}}{d_1}\right) + \mathbf{v} = [q_1, \ldots, q_{S-1}]^T. \tag{5.2}$$

Following the logic in (5.2) matrix $\mathbf{A}$ is used to construct the mean of the DRSS model, $\tilde{\mathbf{r}}$,

$$\tilde{\mathbf{r}} = \mathbf{Ar} = 10\eta \log_{10}\left(\frac{\mathbf{d}}{d_1}\right) = [\tilde{r}_1, \ldots, \tilde{r}_{S-1}]^T. \tag{5.3}$$

Using (5.1) and (4.6), the covariance of $\tilde{\mathbf{r}}$ is

$$\mathbf{A\Sigma A}^T = (1-\rho)\sigma^2(\mathbf{I}_{S-1} + \mathbf{1}\mathbf{1}^T) \; . \tag{5.4}$$

By the property of linear combinations, since non-correlated RSS is $\mathbf{p} \sim N(\mathbf{r}, \sigma^2\mathbf{I})$ then $\mathbf{q} \sim N(\tilde{\mathbf{r}}, \mathbf{A\Sigma A}^T)$. Thus, the PDF of $\mathbf{q}$ may be shown as [37, 38]

$$f(\mathbf{q}) = \frac{\exp\left\{-\frac{1}{2}(\mathbf{q}-\tilde{\mathbf{r}})^T(\mathbf{A\Sigma A}^T)^{-1}(\mathbf{q}-\tilde{\mathbf{r}})\right\}}{(2\pi)^{\frac{S-1}{2}}|\mathbf{A\Sigma A}^T|^{\frac{1}{2}}} \; . \tag{5.5}$$

This is the PDF function used in the remainder of this chapter for all future calculations.

5.3 MLE algorithm for DRSS measurements

The MLE for DRSS involves taking the Log-Likelihood of (5.5) to get,

$$\mathcal{L} = -\frac{(S-1)\ln(2\pi)}{2} + \frac{\ln|\mathbf{A\Sigma A}^T|}{2} - \frac{(\mathbf{q}-\tilde{\mathbf{r}})^T(\mathbf{A\Sigma A}^T)^{-1}(\mathbf{q}-\tilde{\mathbf{r}})}{2}\,. \tag{5.6}$$

All constants may be ignored because they do not affect the final estimate as maximum value is not dependent on the constants, thus (5.6) simplifies to,

$$\mathcal{L} = -\frac{1}{2}(\mathbf{q}-\tilde{\mathbf{r}})^T(\mathbf{A\Sigma A}^T)^{-1}(\mathbf{q}-\tilde{\mathbf{r}}). \tag{5.7}$$

When $\mathbf{\Sigma}$ has the structure in (4.6), using the Woodbury Matrix Identity [39] to find $(\mathbf{A\Sigma A}^T)^{-1}$ that is,

$$(\mathbf{G}+\mathbf{UHV})^{-1} = \mathbf{G}^{-1} - \mathbf{G}^{-1}\mathbf{U}(\mathbf{H}^{-1}+\mathbf{VG}^{-1}\mathbf{U})^{-1}\mathbf{VG}^{-1}. \tag{5.8}$$

Rewriting (5.4) to fit the form of (5.8) gives,

$$(\mathbf{A\Sigma A}^T)^{-1} = (1-\rho)\sigma^2(\mathbf{I}_{S-1}) - (1-\rho)\sigma^2(\mathbf{1}\mathbf{1}^T) \tag{5.9}$$

For brevity, define $\zeta = (1-\rho)\sigma^2$, where $\mathbf{G} = \zeta\mathbf{I}_{S-1},\ \mathbf{H} = \zeta,\ \mathbf{U} = \mathbf{1}$, and $\mathbf{V} = \mathbf{1}^T$. Therefore,

$$\begin{aligned}(\mathbf{A\Sigma A}^T)^{-1} &= \tfrac{1}{\zeta}\mathbf{I}_{S-1} - \tfrac{1}{\zeta}\mathbf{I}_{S-1}\mathbf{1}(\tfrac{1}{\zeta}+\mathbf{1}^T\tfrac{1}{\zeta}\mathbf{I}_{S-1}\mathbf{1})^{-1}\mathbf{1}^T\tfrac{1}{\zeta}\mathbf{I}_{S-1}\\ &= \tfrac{S}{S\zeta}\mathbf{I} - \tfrac{\mathbf{1}\mathbf{1}^T}{S\zeta}\\ &= \tfrac{1}{S\sigma^2(1-\rho)}(S\mathbf{I}-\mathbf{1}\mathbf{1}^T)\,,\end{aligned} \tag{5.10}$$

where $(\mathbf{A\Sigma A})^{-1}$ is a symmetric matrix with $\frac{S-1}{S(\sigma^2-\sigma^2\rho)}$ along the diagonal, and $\frac{1}{S(\sigma^2-\sigma^2\rho)}$ on the off-diagonal.

$$\arg\min_{z_0}\ (\mathbf{q}-\tilde{\mathbf{r}})^T(\mathbf{A\Sigma A}^T)^{-1}(\mathbf{q}-\tilde{\mathbf{r}}) \tag{5.11}$$

where $\mathbf{q}$ is the differential observed data, $\tilde{\mathbf{r}}$ is the mean differential observed power and $\mathbf{A\Sigma A}^T$ is the covariance of the differential noise. Since no closed-form solution is readily available a grid search method and gradient descent method were used to determine the minimization of (5.11). In order to validate this model data was used from experiment six discussed in Chapter 3.

5.3.1 Proposed MLE-GD algorithm using correlated DRSS.

To find the argument that minimizes (4.5), a first order optimization algorithm, known as a gradient descent method, was used. Define a step size, γ and an initial starting position $[x_0, y_0]$, then the new positions $\hat{x}_0$ and $\hat{y}_0$ in the descent are given in (4.5).

To speed up the implementation of the algorithm, (5.11) is expanded and like terms are combined. This closed-form model allows us to numerically evaluate the gradient descent for any $\mathbf{q}$, $\tilde{\mathbf{r}}$ to approximate the argument minimizing (x_0, y_0) for the MLE. As mentioned before, coefficients are absorbed by the step size coefficient, giving,

$$\begin{aligned}\mathcal{L} &= (\mathbf{q}^T(\mathbf{A\Sigma A}^T)^{-1} - \tilde{\mathbf{r}}^T(\mathbf{A\Sigma A}^T)^{-1})(\mathbf{q} - \tilde{\mathbf{r}}) \\ &= \mathbf{q}^T(\mathbf{A\Sigma A}^T)^{-1}\mathbf{q} - 2\mathbf{q}^T(\mathbf{A\Sigma A}^T)^{-1}\tilde{\mathbf{r}} + \tilde{\mathbf{r}}^T(\mathbf{A\Sigma A}^T)^{-1}\tilde{\mathbf{r}}.\end{aligned} \tag{5.12}$$

In order to use the gradient descent method to find the location, the partial derivatives with respect to x_0 and y_0 are needed. Begin by expanding (5.12) around $(\mathbf{A\Sigma A}^T)^{-1}$. Next, lumping the coefficient $(S\sigma^2(1-\rho))^{-1}$ with the step size coefficient and beginning with the first term gives,

$$\mathbf{q}^T(\mathbf{A\Sigma A}^T)^{-1}\mathbf{q} = \mathbf{q}^T(S\mathbf{I} - \mathbf{1}\mathbf{1}^T)\mathbf{q}. \tag{5.13}$$

When taking the derivative with respect to z_0 only terms containing $\tilde{\mathbf{r}}_s$ will not cancel out in the equation, thus (5.13) will drop out of our final equation. Expansion and simplification of coefficients for the second term in (5.12) yields,

$$-2\mathbf{q}^T(\mathbf{A\Sigma A}^T)^{-1}\tilde{\mathbf{r}} = -2\mathbf{q}^T(S\mathbf{I} - \mathbf{1}\mathbf{1}^T)\tilde{\mathbf{r}} \tag{5.14}$$

$$= -2\mathbf{q}^T(S\mathbf{I}\tilde{\mathbf{r}} - \mathbf{1}\mathbf{1}^T\tilde{\mathbf{r}}) \tag{5.15}$$

$$= 1 - 2S(\mathbf{q}^T\tilde{\mathbf{r}}) + 2(\mathbf{q}^T\mathbf{q})(\mathbf{q}^T\tilde{\mathbf{r}}) \tag{5.16}$$

$$= -2S\sum_{s=1}^{S-1} q_s\tilde{r}_s + 2\sum_{s=1}^{S-1} q_s \sum_{s=1}^{S-1}\tilde{r}_s. \tag{5.17}$$

Equation (5.14) is saved for use in the final MLE. The third term is expanded and simplified to yield

$$\tilde{\mathbf{r}}^T(\mathbf{A}\boldsymbol{\Sigma}\mathbf{A}^T)^{-1}\tilde{\mathbf{r}} = \tilde{\mathbf{r}}^T(S\mathbf{I} - \mathbf{1}\mathbf{1}^T)\tilde{\mathbf{r}} \tag{5.18}$$

$$= S(\tilde{\mathbf{r}}^T\tilde{\mathbf{r}}) - (\tilde{\mathbf{r}}^T\mathbf{I})(\mathbf{1}^T\tilde{\mathbf{r}}) \tag{5.19}$$

$$= S\sum_{s=1}^{S-1}\tilde{r}_s^2 - \sum_{s=1}^{S-1}\tilde{r}_s\sum_{s=1}^{S-1}\tilde{r}_s. \tag{5.20}$$

Combining (5.14)-(5.18) and canceling like terms gives (5.21), which can be broken into four terms:

$$\mathcal{L} = \underbrace{-2S\sum_{s=1}^{S-1}q_s\tilde{r}_s}_{\text{A}} + \underbrace{2\sum_{s=1}^{S-1}\tilde{r}_s\sum_{s=1}^{S-1}q_s}_{\text{B}} + \underbrace{S\sum_{s=1}^{S-1}\tilde{r}_s^2}_{C} - \underbrace{\sum_{s=1}^{S-1}\tilde{r}_s\sum_{s=1}^{S-1}\tilde{r}_s}_{\text{D}}. \tag{5.21}$$

The next step in gradient descent involves finding the partial derivative of (5.21). Compute the partial derivative of $\tilde{r}_s$ with respect to x_0 for each $s \in \{1, \cdots, S-1\}$

$$\frac{\partial\tilde{r}_s}{\partial x_0} = \eta\exp_{dB}\left(\frac{x_1 - x_0}{d_1^2} - \frac{x_s - x_0}{d_s^2}\right). \tag{5.22}$$

Similarly, the partial derivative of $\tilde{r}_s$ with respect to y_0 is

$$\frac{\partial\tilde{r}_s}{\partial y_0} = \eta\exp_{dB}\left(\frac{y_1 - y_0}{d_1^2} - \frac{y_s - y_0}{d_s^2}\right). \tag{5.23}$$

The coefficient part of (5.21) can be lumped in with the step size. The partial derivative $\frac{\partial\mathcal{L}}{\partial x_0}$ can be broken up as,

$$\frac{\partial A}{\partial x_0} = \frac{\partial}{\partial x_0}\left(-2S\sum_{s=1}^{S-1}q_s\tilde{r}_s\right) = -2S\sum_{s=1}^{S-1}q_s\frac{\partial\tilde{r}_s}{\partial x_0} \tag{5.24}$$

$$\frac{\partial B}{\partial x_0} = \frac{\partial}{\partial x_0}\left(2\sum_{s=1}^{S-1}\tilde{r}_s\sum_{t=1}^{S-1}q_t\right) = 2\sum_{t=1}^{S-1}q_t\sum_{s=1}^{S-1}\frac{\partial\tilde{r}_s}{\partial x_0} \tag{5.25}$$

$$\frac{\partial C}{\partial x_0} = \frac{\partial}{\partial x_0}\left(S\sum_{s=1}^{S-1}\tilde{r}_s^2\right) = 2S\sum_{s=1}^{S-1}\tilde{r}_s\frac{\partial\tilde{r}_s}{\partial x_0} \tag{5.26}$$

$$\frac{\partial D}{\partial x_0} = \frac{\partial}{\partial x_0}\left(-\sum_{s=1}^{S-1}\tilde{r}_s\sum_{t=1}^{S-1}\tilde{r}_t\right) = -2\sum_{s=1}^{S-1}\frac{\partial\tilde{r}_s}{\partial x_0}\sum_{t=1}^{S-1}\tilde{r}_t\,. \tag{5.27}$$

Combining (5.24)-(5.27) gives,

$$\frac{1}{2}\frac{\partial \mathcal{L}}{\partial x_0} = S\sum_{s=1}^{S-1}(\tilde{r}_s - q_s)\frac{\partial \tilde{r}_s}{\partial x_0} + \sum_{t=1}^{S-1}(q_t - \tilde{r}_t)\sum_{s=1}^{S-1}\frac{\partial \tilde{r}_s}{\partial x_0}. \tag{5.28}$$

The gradient with respect to y is, similarly, determined to be

$$\frac{1}{2}\frac{\partial \mathcal{L}}{\partial y_0} = S\sum_{s=1}^{S-1}(\tilde{r}_s - q_s)\frac{\partial \tilde{r}_s}{\partial y_0} + \sum_{t=1}^{S-1}(q_t - \tilde{r}_t)\sum_{s=1}^{S-1}\frac{\partial \tilde{r}_s}{\partial y_0}, \tag{5.29}$$

where $\tilde{r}_s$ is the differential power from the transmitter to receiver s, q_s is the observed differential data and S is the number of receivers. Using Telos-B data, (5.28) and (5.29) validations were performed.

5.4 Experimental validation of this author's DRSS MLE-GD algorithm

Experimental data from Chapter 3 was used to validate the DRSS model using a MLE-GD algorithm. As mentioned in the correlated fading model, (4.10), assume $\eta = 1$ for this model. Since the P_0 values cancel out in the DRSS power measurements, its values are trivial.

Figure 5.1 shows the RMSE for the estimated transmitter location assuming a DRSS model and using data obtained with the Telos-Bs, for noise variance values of $\sigma^2 = 16, 64,$ and 100. For a A straight line was fit to the RSS measurements found in experiment six in Chapter 2 in order to estimate P_0 and η. The estimated variables of this equation gave $P_0 = 43\,dBm$ and $\eta = 1$. Thus, these were the parameters used in the algorithm estimation. It is shown in Figure 5.1 that for a noise variance of sixteen the algorithm generally performs better than with a higher variance. As the correlation values increase the RMSE initially drops and then evens out for $\sigma^2 = 16$. When noise fading variance is increased ($\sigma^2 = 64, 100$) the RMSE becomes less stable and may require a greater number of iterations to converge. The DRSS model is able to achieve a RMSE value of as low as 2.5 feet when lower noise fading variance values are used. This might suggest that the DRSS model is best suited for low noise measurements that are highly correlated.

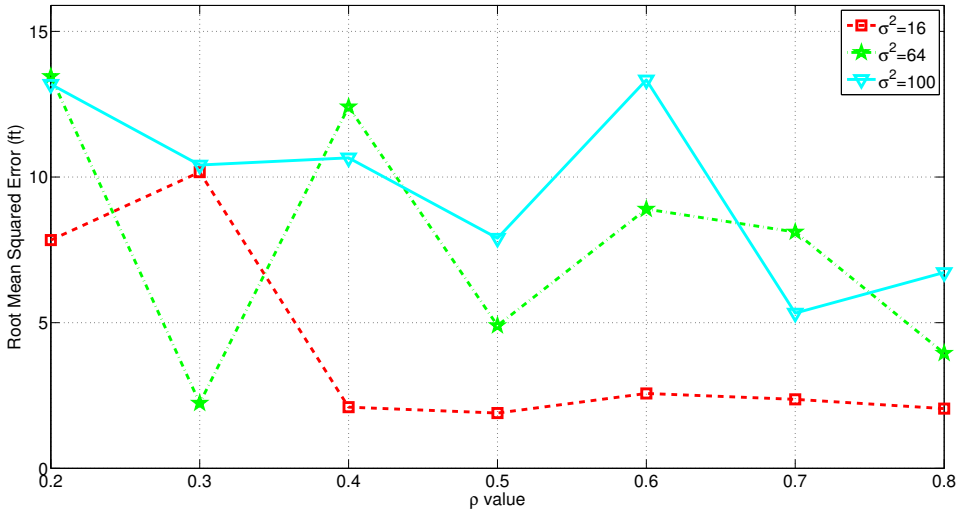

Figure 5.1: Experimental error versus correlation for the estimated transmitter location assuming a DRSS model, using measurements obtained from experiment six in Chapter 3 and localized using a gradient descent algorithm. The squares correspond to $\sigma^2 = 16$, the stars correspond to $\sigma^2 = 64$ and the triangles correspond to $\sigma^2 = 100$.

Figure 5.2 on page 64, compares experimental error using Telos-B measurements for the correlated DRSS MLE-GD, correlated MLE-GRID and correlated DRSS MLE-grid, assuming an $\eta = 1$, and $P_0 = 43$ as found in Chapter 4. This graph was used to validate these algorithms, as ρ increases from 0.2 to 0.5 the MLE-GRID algorithm has the best performance. These values correspond to lower correlation assumptions. Given the environment in which these measurements were taken (Kenney Hall), it is reasonable to assume that measurements would have a medium to high correlation coefficient. If this is true, it would mean that a low correlation coefficient is an inaccurate assumption. At medium to high correlation values ($0.5 \geq \rho \leq 0.8$), both of the DRSS algorithms locate the transmitter with more accuracy than the RSS model. The MLE-GD algorithm performs slightly better than the MLE-GRID algorithm. With $\rho = 0.6$ an experimental error of 2.49 feet is achieved with the MLE-GD algorithm. An error of 2.57 feet was achieved with the MLE-GRID algorithm, while the correlated MLE has an experimental error of 6.9 feet.

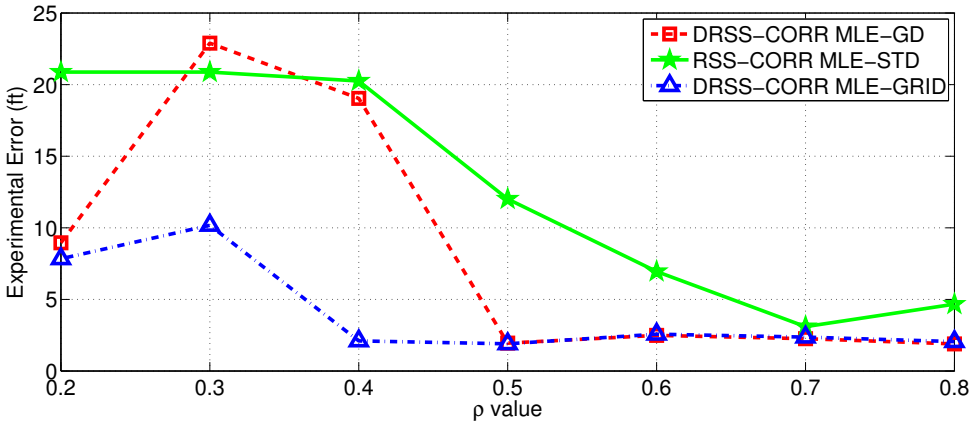

Figure 5.2: Experimental error versus correlation for the estimated transmitter location $(16, 16)$ assuming a DRSS model with a gradient descent algorithm (red dash square), correlated RSS MLE-grid (green x) and correlated DRSS MLE-grid using measurements obtained from experiment six in Chapter 3

.

Using the data from experiment six in Chapter 3, it was shown that the DRSS algorithm performs better than the correlated RSS algorithm. This is likely due to the fact that transmit power is trivial for DRSS measurements and therefore has no bearing on the algorithms for DRSS, while the algorithms used with correlated RSS are dependent on the assumption of P_0. Thus, whenever possible, DRSS algorithms should be considered to localize a Telos-B mote as in a situation similar to this author's experimental set-up. This can produce estimates which are within two feet of the actual location of the transmitter.

5.5 Complexity Analysis for MLE algorithms using DRSS measurements

When analyzing the performance of an algorithm it is not only important to consider the RMSE, but also the computational complexity of each algorithm. For instance, an algorithm that performs only slightly better, but takes twice as long computationally would not be desired.

When considering Table 5.1, it is important to remember that each operation must be performed for each grid point that the algorithm must search across and for each iteration of the gradient descent algorithm. For a search space of $-20 : 10 : 20$ (i.e. the algorithm

Table 5.1: Complexity table to compare the number of operations it takes for each algorithm to run. Note this is per grid point or per iteration for rows one and two, respectively.

Algorithm	×	±	÷	Log
MLE GRID	13S	9S	0	S
MLE GD	13S	8S	S	S

will look at only five points between $(-20, -20)$ and $(20, 20)$) and with five iterations of the MLE-GD, it would take the algorithms about the same amount of time to run. However, the search space that the MLE-GRID algorithm has to use is much coarser and results in higher estimation errors.

5.6 Simulations for MLE algorithms using DRSS measurements

This author was interested in investigating the performance of three different models of signal strength: (1) correlated RSS using a MLE-GRID algorithm, (2) correlated DRSS using a MLE-GRID based algorithm and (3) correlated DRSS using a MLE-GD algorithm. Unless stated otherwise in the caption, the following parameters are assumed to be known for each case: $S = 36$, $16 \leq \sigma^2 \leq 122$ which encompasses most generally used values of the noise term, search space $= [-20 : 2 : 20] \times [-20 : 2 : 20]$, $P_0 = 20\,dB$, $0.2 \leq \rho \leq 0.8$ and $(x_0, y_0) = (-5.5, 7.5)$. The algorithms are all initiated at $(x, y) = (1, 1)$ and 1000 trials were run for each choice of ρ. Starting with a step size of $\gamma = 0.001$ then (4.5) becomes

$$\hat{x}_0 = x - \gamma \left(S \sum_{s=1}^{S-1} (\tilde{r}_s - q_s) \frac{\partial \tilde{r}_s}{\partial x_0} + \sum_{t=1}^{S-1} (q_t - \tilde{r}_t) \sum_{s=1}^{S-1} \frac{\partial \tilde{r}_s}{\partial x_0} \right). \tag{5.30}$$

The equation for $\hat{y}_0$ is similar. Figure 5.3 shows that as correlation increases the MLE-GD performs better than any of the other algorithms in terms of RMSE. Results for three different variances are shown and $\sigma^2 = 16$ gives the most accurate estimate of the transmitter location. For $\rho = 0.8$ the experimental error of the transmitter location is

2.05 feet. When $\rho = 0.5$ the RMSE is 1.9 feet. This leads to the conclusion that when measurements are highly correlated, $\rho = 0.8$, the estimated location of the transmitter (which is actually located at $(16, 16)$ feet) is accurate to within two feet. Both of these values of experimental error are lower than the same model that was run using the well-known correlated fading model.

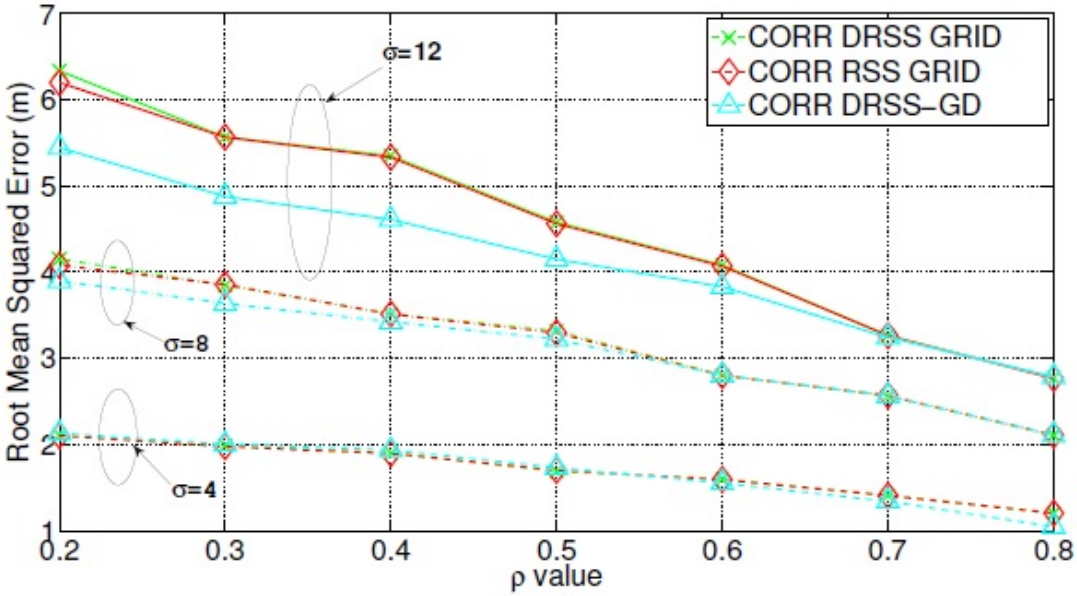

Figure 5.3: RMSE error versus ρ value for $\sigma^2 = 16, 64, 122$. When the parameters are adjusted for optimal performance, (dense grid, large number of iterations).

In almost all cases shown in Figure 5.4 the RMSE for the MLE which uses gradient descent is lower than that for other methods. As the correlation coefficient increases, the overall RMSE decreases. This may be due to the fact that as the correlation coefficient increases the measurements come closer to being perfectly correlated $\rho = 1$, so there is less and less of a difference in degrees of freedom in the correlated noise. As expected, as the noise term σ^2 increases, the RMSE increases. The optimal conditions for MLE-GD to perform well are high correlation with low noise, although its performance is superior to the other algorithms regardless of the level of noise or correlation value. For any given simulation, the MLE-GRID algorithm and CORR RSS MLE algorithm perform similarly.

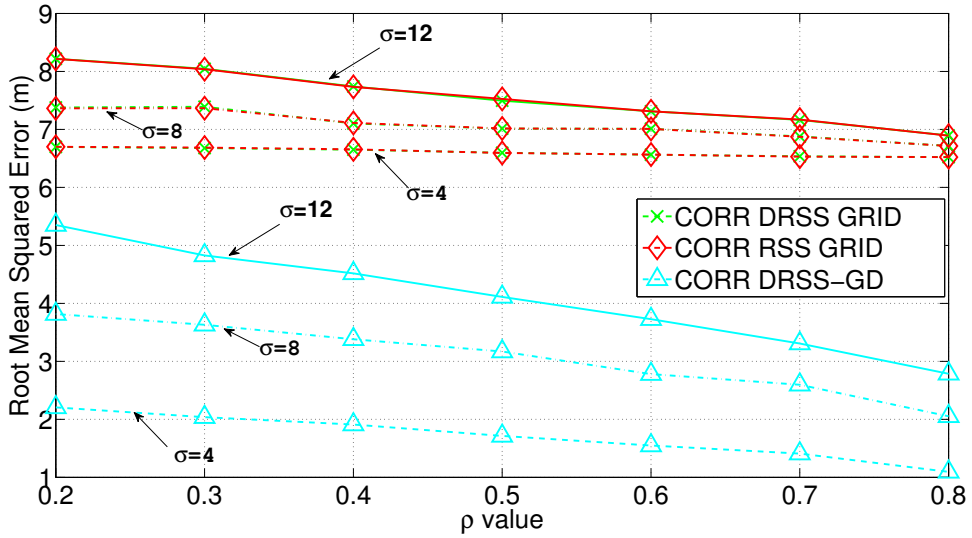

Figure 5.4: RMSE versus ρ value for $\sigma^2 = 16, 64, 122$. Results when algorithms take approximately the same number of operations.

If the algorithms are forced to compute in the same amount of time, the gradient descent algorithm is more accurate than either of the other algorithms, even in high noise cases. This is likely due to the fact that there is such a coarse search space for both of the other models because they both use a MLE-GRID as opposed to the MLE-GD.

5.6.1 Conclusions on the proposed single transmitter DRSS model and algorithm.

A novel MLE-GD algorithm to estimate the location of a transmitter by using correlated DRSS measurements was proposed and it was shown that the MLE-GD algorithm for the correlated shadowing DRSS model is more accurate than that of the grid search algorithm. For fine levels of resolution the MLE-GD algorithm also requires less time computationally than the grid search algorithm. There is not a significant difference in the performance of the correlated RSS and correlated DRSS MLE-GRID algorithms. When the MLE-GD and MLE-GRID algorithms perform the same number of operations, the MLE-GRID produces RMSE errors that are sometimes three times higher than that of the MLE-GD algorithm. Due the MLE-GD being the more accurate and less time consuming option, it is the preferred method for localization of a transmitter. Further research into this topic would involve comparing results to real world RSS data and extending the model

to account for multiple transmitters. To this author's knowledge no current literature uses correlated DRSS measurements with a gradient descent algorithm to locate a transmitter, but it has been validated, through experimental data and simulations, that it is a better alternative to the standard MLE-GRID algorithm.

5.7 Development of a DRSS model for multiple transmitters (DRSS-M)

To the author's knowledge, no literature currently exists which uses correlated DRSS measurements to localize multiple transmitters. This section combines Nelson's quasi-EM [26] algorithm with our simple DRSS model. The adjusted DRSS model, denoted as DRSS-M would be:

$$R_{sm} = \frac{P_0}{d_s(z_m)^{\eta}}, \tag{5.31}$$

$$P_s = \sum_{m=1}^{M} R_{sm} + w_s, \tag{5.32}$$

where $w_s \sim N(\mathbf{0}, \mathbf{\Sigma})$, $d_s(z_m)$ denotes the distance from receiver s to transmitter m, R_{sm} is the noise free RSS measurements from receiver s to transmitter m and $\tilde{r}_{(sm}$ are the RSS noise free measurements from the difference of receiver one minus all other receivers and thus is a $(S-1) \times M$ matrix. From (5.31) define a PDF of the correlated DRSS measurements received from multiple transmitters as,

$$f(\mathbf{q}) = \frac{1}{(2\pi|\mathbf{\Sigma}|)^{S/2}} \exp\left[-(\mathbf{q}-\tilde{\mathbf{r}})^T(\mathbf{A}\mathbf{\Sigma}\mathbf{A}^T)^{-1}(\mathbf{q}-\tilde{\mathbf{r}})\right], \tag{5.33}$$

where S is the number of new receivers $s = 1, \cdots, S-1$. In order to perform a MLE, first find the log-likelihood function of (5.33) and then maximize it. Ignoring all constants that will drop out during the derivation,

$$\mathcal{L} = -\left(\mathbf{q} - \sum_{s=2}^{S} \tilde{\mathbf{r}}_s\right)\left(\mathbf{q} - \sum_{s=2}^{S} \tilde{\mathbf{r}}_s\right)^T. \tag{5.34}$$

The EM technique described in Chapter 4 cannot be used with (5.34) and therefore an adaptation of the quasi-EM was used to localize the transmitters.

To this author's knowledge, multiple DRSS localization has not been researched in the literature and therefore no standard of model exists. Thus, it is necessary to derive a quasi-EM algorithm based on some of the research performed by Nelson et al. Referring back to (2.23) define the RSS as,

$$P_s = \sum_{m=1}^{M} R_{sm} 10^{w_{ms}/10}, \tag{5.35}$$

where R_{sm} is the linear RSS value for the multiple transmitters and $\mathbf{w} \sim N(\mathbf{0}, \mathbf{\Sigma})$. The following five steps can be followed to implement the quasi-EM algorithm.

Step 1 Generate M initial position estimates for the transmitters, $\hat{z}_m$ from a uniform distribution within a specified search space.

Step 2 Given the current estimate derived in Step 1 determine the expected RSS power at the sth receiver from the m^{th} transmitter

$$E_{ms} = \left(\frac{P_0 d_0^{\eta}}{d_s(\hat{z}_m)^{\eta}} \right) , \tag{5.36}$$

where P_0 is the transmit power, d_0 is the close-in reference distance, generally taken to be one meter and $d_s(\hat{z}_m)$ is the distance from the estimated location of the m^{th} transmitter to the s^{th} receiver. Even though P_0 is used, it drops out in the next step, so for DRSS any dummy variable can be used.

Step 3 Normalize powers obtained in step two so that they give a total power at each receiver that is equal to the observed power at that receiver,

$$\tilde{E}_{ms} = \frac{P_s E_{ms}}{\sum_{m=1}^{M} E_{ms}} \tag{5.37}$$

$$\tilde{e}_{ms} = 10 \log_{10}(\tilde{E}_{ms}) , \tag{5.38}$$

where P_s is the total power from receiver s and E_{ms} is the normalized power.

Step 4A In order to compute the DRSS, take the difference of the RSS measurements and a reference receiver (defined as receiver 1),

$$\Delta_{ms} = \tilde{e}_{m1} - \tilde{e}_{ms} \tag{5.39}$$

$$= 10\log_{10}\left(\frac{d_s(\hat{z}_m)^\eta}{d_1(\hat{z}_m)^\eta}\right) + (w_{m1} - w_{ms}). \tag{5.40}$$

Step 4B Using Δ_{ms} from Step 3, re-estimate transmitter locations by minimizing sum of squared error, given by

$$\hat{z}_m = \arg\min_{z_0} \sum_{s=1}^{S} \left(\Delta_{ms} - \frac{d_s(\tilde{z}_m)^\eta}{d_1(\tilde{z}_m)^\eta}\right)\left(\mathbf{A\Sigma A}^T\right)^{-1}\left(\Delta_{ms} - \frac{d_s(\tilde{z}_m)^\eta}{d_1(\tilde{z}_m)^\eta}\right)^T , \tag{5.41}$$

where Δ_{ms} is the normalized total power, $d_s(\tilde{z}_m)$ is the distance from the estimated transmitter locations to receiver s and $d_1(\tilde{z}_m)$ is the distance from the reference receiver one to transmitter m.

Step 5 Repeat Steps 2-4 for a set number of iterations. Due to the quasi-EM algorithm's failure to converge to a local minimum after only a single iteration, it was run multiple times with different random initial conditions. A cost function is used to find the initialization that yields the lowest sum of squared log-power error.

$$C(\hat{z}) = \sum_{s=1}^{S}\left(\Delta_{ms} - \log_{10}\left(\frac{d_s(\hat{z}_m)^\eta}{d_1(\hat{z}_m)^\eta}\right)\right)^2 , \tag{5.42}$$

where P_s is the observed power at the s^{th} receiver, $d_s(\hat{z}_m)$ is the distance from the final estimate of transmitter m to receiver s, $d_1(\hat{z}_m)$ is the distance from the reference receiver one to estimated transmitter location s and η is the path loss exponent.

5.7.1 Simulations for multiple transmitter DRSS (DRSS-M).

Simulations were performed to investigate the actual (x_m, y_m) and path that is taken by each of the four initialization to get to the estimated $(\hat{x}_m, \hat{y}_m)$ using the MLE-EM function

for DRSS-M for $S = 144$ receivers, with $\sigma^2 = 16$, Figure 5.5. For all simulations $\eta = 2$, $\sigma^2 = 4$ or $\sigma^2 = 16$, $d_0 = 1$ meter, $0.2 < \rho < 0.8$, reference receiver $s = 1$ and receiver spacing of 10 meters is used. The simulation assumes correlated noise.

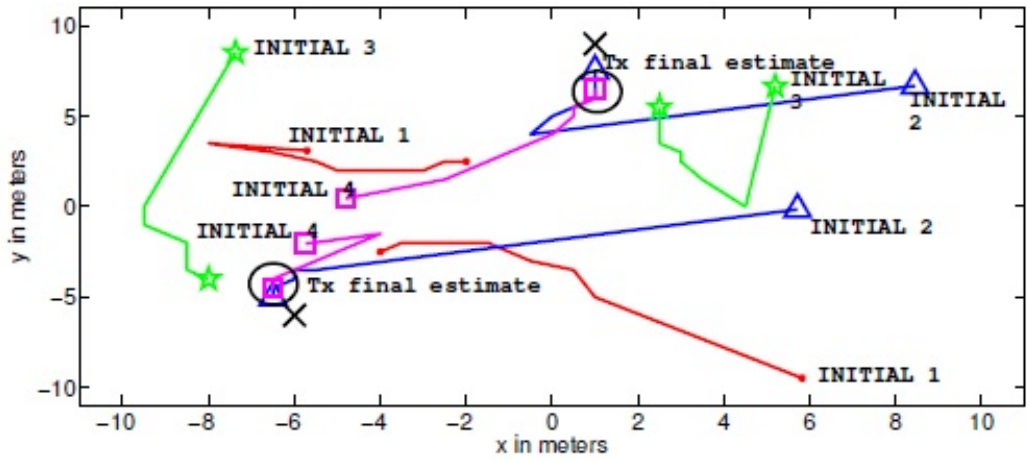

Figure 5.5: Actual (x_m, y_m) and path that is taken by each of the four initialization to get to the estimated $(\hat{x}_m, \hat{y}_m)$ using the MLE-EM function for DRSS-M for $S = 144$ receivers, with $\sigma^2 = 16$. The algorithm also uses a cost function to find the best initialization which is indicated by a black circle. True transmitter location is indicated by a **x** and final estimated transmitter position is contained in the circle. The first initialization is represented by a dot, the second initialization is represented by a star, initialization three is represented by a triangle and the fourth initialization is represented by a square.

The proposed multiple transmitter DRSS model with $\sigma^2 = 16$ estimates transmitter one to be at $(1, 6.5)$ and transmitter two to be at $(-6.5, -4.5)$. All initializations appear to be converging to a local minimum. However, more iterations or initializations may be necessary as the algorithm has a tendency to get stuck at a local minimum. Simulations were also run for $S = 4, 16, 36, 64$ and 100 with $\sigma^2 = 4$, 16 and are included in the

Appendix, Chapter 7. The cost function finds the most accurate initialization. Additionally, all initializations appear to be converging to the same local minimum. Since multiple transmitter DRSS is an unexplored topic in the literature, there is not another algorithm to use for comparison. Future research endeavors could include developing a MLE-GD algorithm for multiple transmitter DRSS.

5.7.2 Experimental validation of DRSS multiple transmitter localization.

As mentioned before, WARP boards acted as transmitters and a Wi-Pry was the receiver. A $\eta = 1.3$ was used because measured path-loss generally varied between one and two.

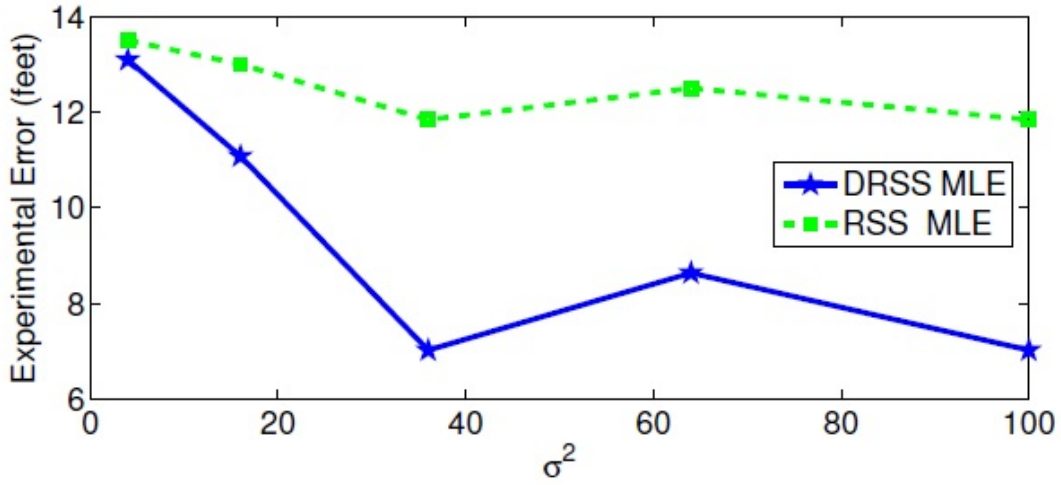

Figure 5.6: Experimental error versus $\sigma^2 = 4, 16, 36, 64, 100$ for multiple transmitter DRSS and RSS algorithms assuming $\rho = 0$. This is just one experimental data set that was used in order to validate the DRSS multiple transmitter algorithm.

Figure 5.6 shows the RMSE measurements versus $\sigma^2 = 4, 16, 36, 64, 100$ assuming $\rho = 0$ when using the DRSS multiple transmitter algorithm. RMSE is lowest for DRSS-M estimates when noise fading variance is $\sigma^2 = 36$. At this variance an RMSE of around 7 feet was obtained for both transmitters using a DRSS-M model, while the RSS-M model

produced an error of 13 feet. For all of the noise fading variance values the RMSE for the DRSS-M model was lower than that of the RSS-M model.

5.7.3 Conclusions on proposed DRSS-M model and algorithm.

The DRSS-M model is more accurate model when considered over the RSS-M model for localization of multiple transmitters. A quasi-expectation maximization (MLE-QEM) algorithm was used for simulations and it was shown that the DRSS-M was sometimes 80% more accurate than its RSS-M counterpart for locating multiple transmitters. Again, this likely due to the absence of a transmit power value for the DRSS-M model and equation. Using DRSS-M measurements for multiple transmitters is a new field of research so this area is wide open to continue performing research. There are a number of topics for future research including, but not limited to, different algorithms, testing environments, experimental equipment and varying the correlation coefficient.

VI. Conclusions, Future Work, and Publications

6.1 Conclusions and Future Work

The research in this dissertation was focused on investigating existing RSS models and algorithms. The purpose was to identify sources of error in current models and develop models and algorithms that are cost efficient and computationally simple. A review of the literature showed the importance of considering an appropriate model for RSS data. To address issues with factors such as number of antennas, transmitters and noise, this author proposed a RSS-GMM, DRSS-M, DRSS-CORR and RSS-CORR model.

This author conducted an experimental campaign described in Chapter 3 to provide real world experiments using a variety of receivers and transmitters. The research provided data regarding the importance of parameter characterization before localization implementation. A novel way to compare experiments is presented to assess the ability of the hardware to report consistent and reliable measurements. The author developed the following algorithms: MLE-NC, MLE-COOP, MLE-GD, MLE-QEM and MLE-GMM. It was shown that when a MLE-STD is used to estimate the location of non-cooperative data there is overconfidence in accuracy of estimates. It was shown that an MLE-GD is a superior algorithm compared to the MLE-GRID. A new model (DRSS-M) and algorithm (MLE-QEM) were developed. Findings provide evidence that DRSS measurements perform approximately 84% better than traditional RSS measurements for estimating multiple transmitter locations.

Overall, this dissertation showed the importance of properly modeling data. Several new models, RSS-GMM, DRSS-CORR and DRSS-M were developed. In addition to developing algorithms for the new models (MLE-GMM, MLE-GD and MLE-QEM), novel algorithms for previously established models MLE-NC and MLE-COOP were developed.

The models and algorithms described in this dissertation could be used in signal processing localization when it is desirable to use RSS measurements. Future work that could extend this dissertation could include further investigation into DRSS measurements, specifically, trying other algorithms, looking at correlation in the path-loss and localization when the location of the receivers is not known. Additional data could also be collected from different environments using different equipment. Combining models may also be of interest, for instance, looking at a non-cooperative multiple transmitter model and corresponding algorithms.

6.2 Contributions

- Statistical analysis of various hardware.
- Models and associated MLE's :
  - Cooperative RSS using a grid search MLE algorithm [6],[40].
  - Non-cooperative RSS with a grid search MLE algorithm [6],[40].
  - Multi-antenna RSS or (GMM) with a grid search algorithm.
  - Correlated RSS, with a grid search algorithm.
  - DRSS with correlation in the RSS values using a gradient descent.
  - Multiple transmitter DRSS using a quasi-EM algorithm.
- Recommendations on model use:
  - It was shown that using the wrong model leads to false performance prediction [6], [40], [41].
  - It was shown that assuming a standard model when the model is actually non-cooperative leads to overconfidence in low RMSE values.
  - Assuming a standard model when the model is actually a GMM leads to large errors.

VII. Appendix

This Appendix provides the additional graphs that were discussed in Chapter 5 for multiple transmitters. The graphs show the path that each initialization of the algorithm took in order to get to its final estimate. The best estimate as determined by the cost function is indicated by the circle.

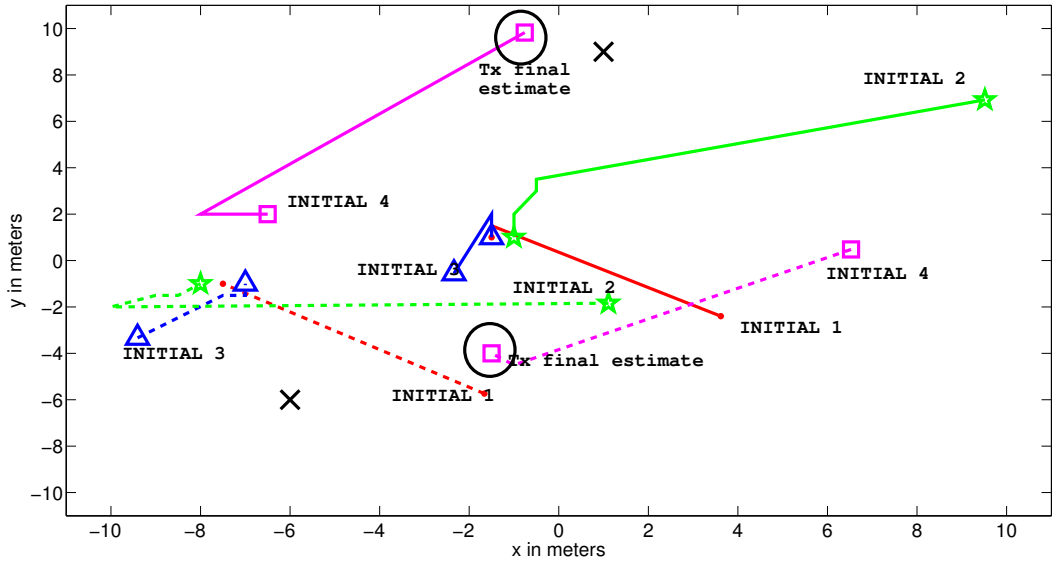

Figure 7.1: Iterations taken for four initializations of a MLE algorithm which used multiple transmitter DRSS from measurements at $S = 4$ receivers, with $\sigma^2 = 4$. The algorithm also uses a cost function to find the best initialization which is indicated by a black circle.

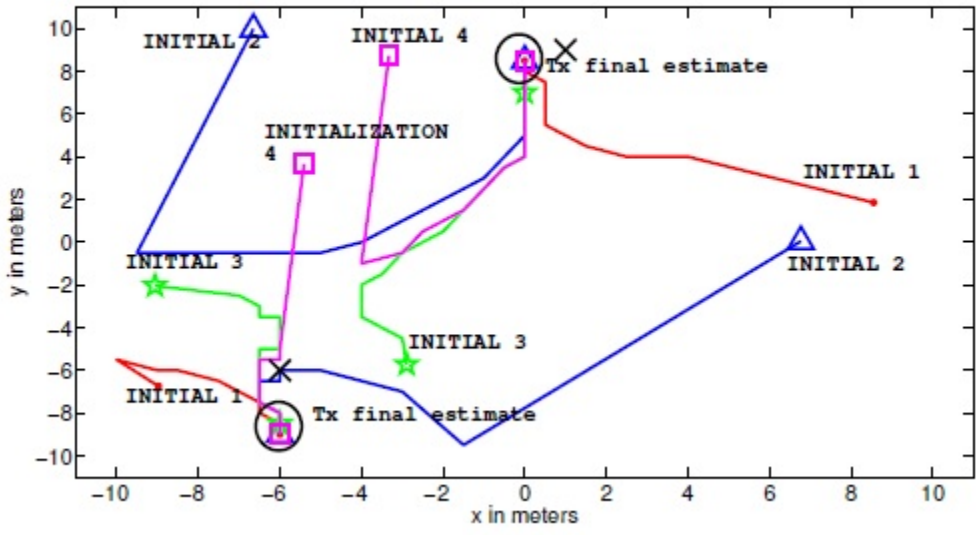

Figure 7.2: Iterations taken for four initializations of a MLE algorithm which used multiple transmitter DRSS from measurements at $S = 16$ receivers, with $\sigma^2 = 4$. The algorithm also uses a cost function to find the best initialization which is indicated by a black circle.

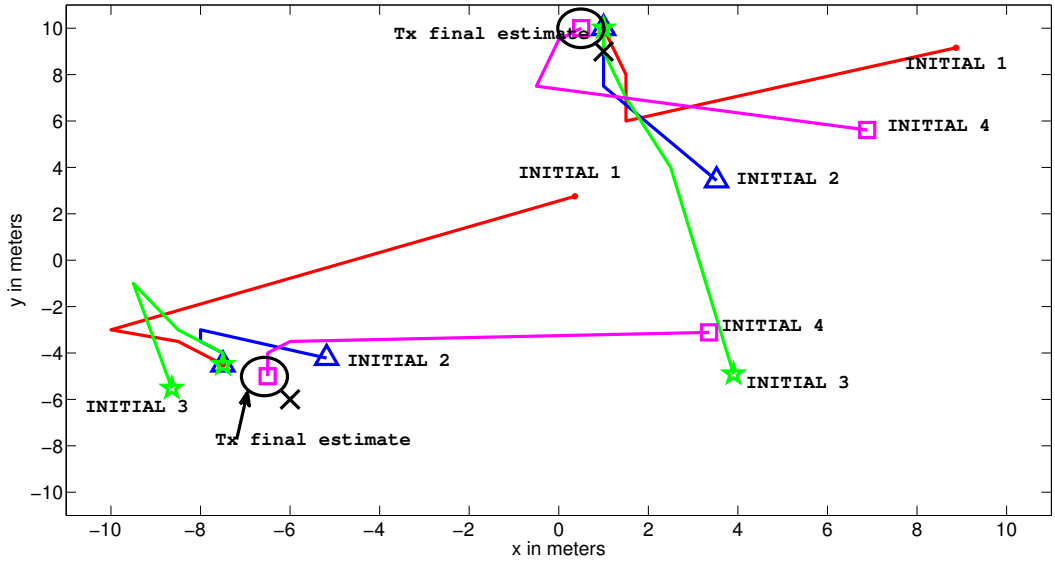

Figure 7.3: Iterations taken for four initializations of a MLE algorithm which used multiple transmitter DRSS from measurements at $S = 36$ receivers, with $\sigma^2 = 4$. The algorithm also uses a cost function to find the best initialization which is indicated by a black circle.

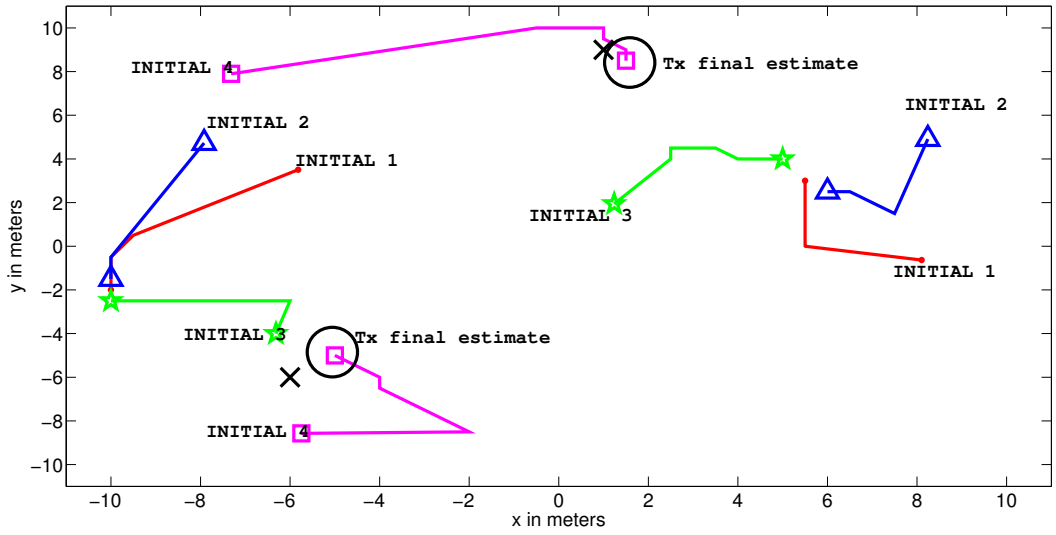

Figure 7.4: Iterations taken for four initializations of a MLE algorithm which used multiple transmitter DRSS from measurements at $S = 64$ receivers, with $\sigma^2 = 4$. The algorithm also uses a cost function to find the best initialization which is indicated by a black circle.

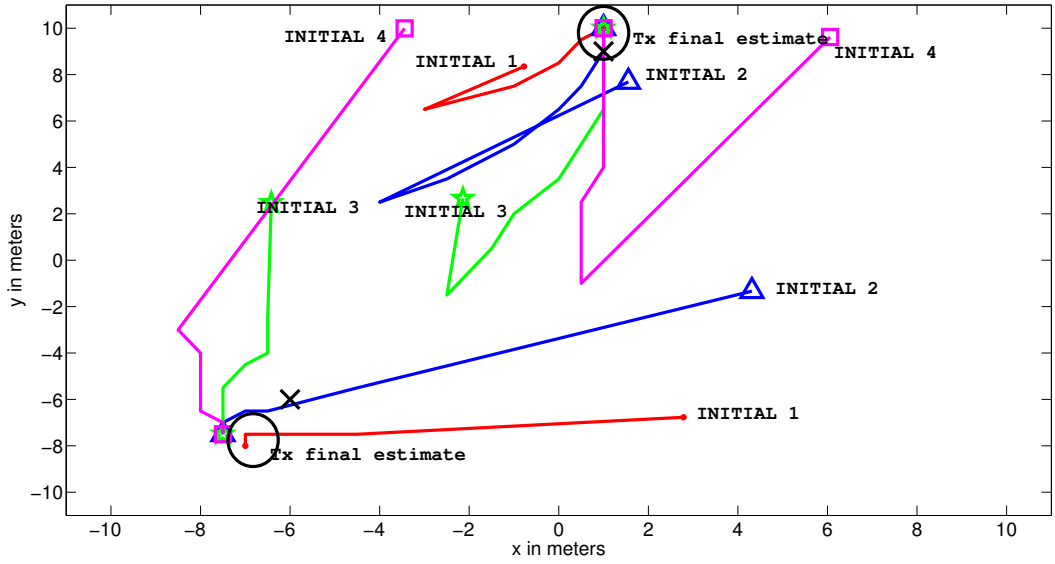

Figure 7.5: Iterations taken for four initializations of a MLE algorithm which used multiple transmitter DRSS from measurements at $S = 100$ receivers, with $\sigma^2 = 4$. The algorithm also uses a cost function to find the best initialization which is indicated by a black circle.

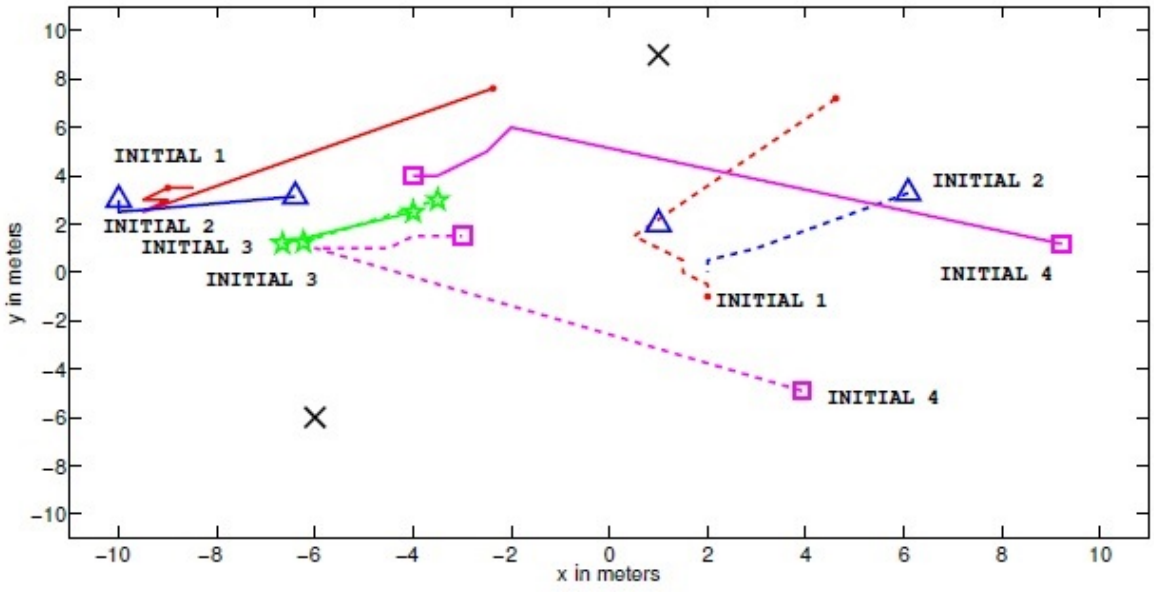

Figure 7.6: Iterations taken for four initializations of a MLE algorithm which used multiple transmitter DRSS from measurements at $S = 4$ receivers, with $\sigma^2 = 16$. The algorithm also uses a cost function to find the best initialization which is indicated by a black circle.

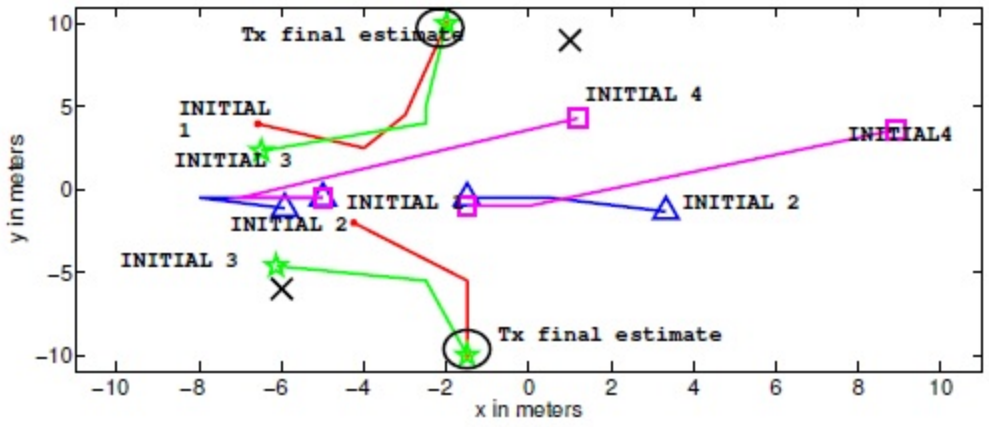

Figure 7.7: Iterations taken for four initializations of a MLE algorithm which used multiple transmitter DRSS from measurements at $S = 16$ receivers, with $\sigma^2 = 16$. The algorithm also uses a cost function to find the best initialization which is indicated by a black circle.

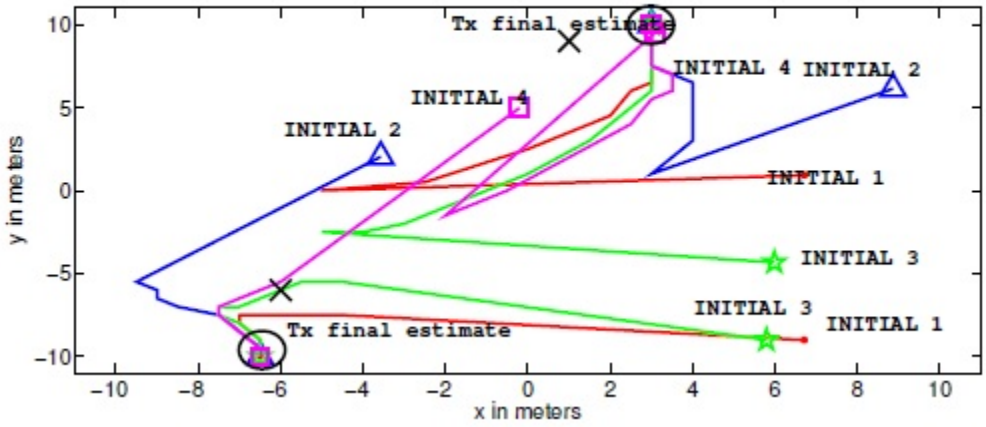

Figure 7.8: Iterations taken for four initializations of a MLE algorithm which used multiple transmitter DRSS from measurements at $S = 36$ receivers, with $\sigma^2 = 16$. The algorithm also uses a cost function to find the best initialization which is indicated by a black circle.

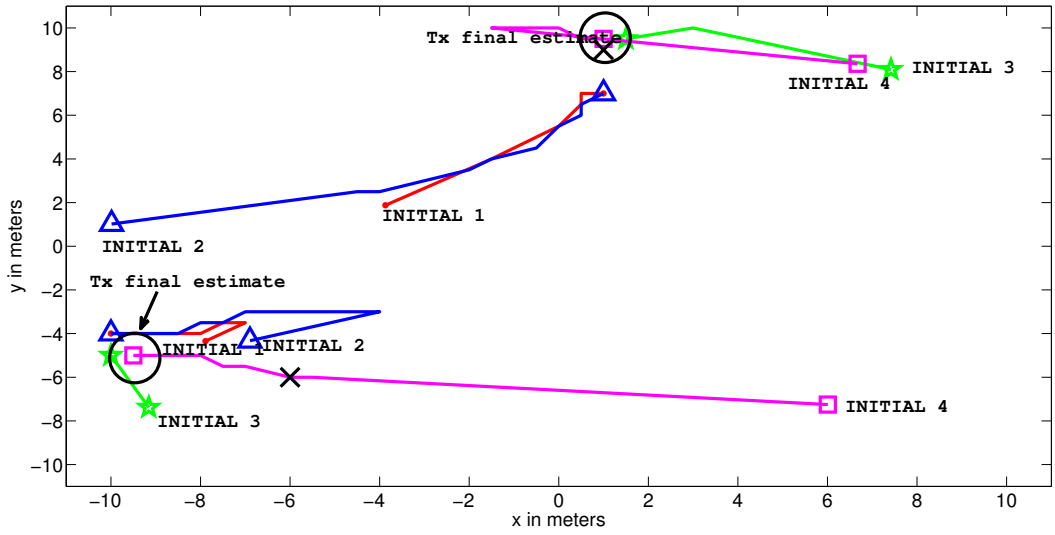

Figure 7.9: Iterations taken for four initializations of a MLE algorithm which used multiple transmitter DRSS from measurements at $S = 100$ receivers, with $\sigma^2 = 16$. The algorithm also uses a cost function to find the best initialization which is indicated by a black circle.

Bibliography

[1] RevLocal, "Location based services project substational revenue growth." http://www.revlocal.com/local-search-news/Local-Search/154_Location-based-services-project-substantial-revenue-growth/.

[2] A. Dogandzic and P. Amran, "Signal-strength based localization in wireless fading channels," in *Signals, Systems and Computers, 2004. Conference Record of the Thirty-Eighth Asilomar Conference on*, vol. 2, pp. 2160 – 2164 Vol.2, Nov. 2004.

[3] P. Tarrio, A. Bernardos, and J. Casar, "An RSS localization method based on parametric channel models," in *Sensor Technologies and Applications, 2007. SensorComm 2007. International Conference on*, pp. 265 –270, Oct. 2007.

[4] Y. Chen and H. Kobayashi, "Signal strength based indoor geolocation," in *Communications, 2002. ICC 2002. IEEE International Conference on*, vol. 1, pp. 436 –439, 2002.

[5] D. Vassis, G. Kormentzas, A. Rouskas, and I. Maglogiannis, "The IEEE 802.11g standard for high data rate WLANs," vol. 19, pp. 21–26, May 2005.

[6] R. Martin, A. King, J. Pennington, R. Thomas, R. Lenahan, and C. Lawyer, "Modeling and mitigating noise and nuisance parameters in received signal strength positioning," *IEEE Transactions on, Signal Processing*, vol. 60, pp. 5451 –5463, Oct. 2012.

[7] N. Patwari, J. N. Ash, S. Kyperountas, A. O. Hero, III, R. L. Moses, and N. S. Correal, "Locating the nodes – cooperative localization in wireless sensor networks," *IEEE Signal Processing Magazine*, vol. 22, no. 4, pp. 54–69, 2005.

[8] N. Salman, M. Ghogho, and A. Kemp, "On the joint estimation of the RSS-based location and path-loss exponent," *IEEE Wireless Communications Letters*, vol. 1, pp. 34 –37, Feb. 2012.

[9] T. Rappaport, *Wireless Communications-Principles and Practice*. Prentice Hall PTR, 1996.

[10] M. Gudmundson, "Correlation model for shadow fading in mobile radio systems," *Electronics Letters*, vol. 27, pp. 2145 –2146, Nov. 1991.

[11] J. Flam, G. Kraidy, and D. Ryan, "Using a sensor network to localize a source under spatially correlated shadowing," in *2010 IEEE 71st Conference on Vehicular Technology (VTC 2010-Spring)*, pp. 1 – 5, May 2010.

[12] A. H. Al-Dhalaan and I. Lambadaris, "Wireless sensor network localization with spatially correlated shadowing," in *2010 IEEE International Conference on Communications (ICC)*, pp. 1 –6, May 2010.

[13] N. Patwari and P. Agrawal, "Effects of correlated shadowing: connectivity, localization, and RF tomography," in *2008 International Conference on Information Processing in Sensor Networks*, pp. 82–93, July 2008.

[14] M. Assad, M. Heidari, and K. Pahlavan, "Effects of Channel Modeling on Performance Evaluation of WiFi RFID Localization Using a Laboratory Testbed," in *2007 IEEE Global Telecommunications Conference*, pp. 366 –370, Nov. 2007.

[15] J. H. Lee and R. M. Buehrer, "Location estimation using differential RSS with spatially correlated shadowing," in *Proceedings of the 28th IEEE Conference on Global Telecommunications*, (Piscataway, NJ, USA), pp. 4613–4618, IEEE Press, 2009.

[16] L. Mailaender, "Received signal strength (RSS) location estimation with nuisance parameters in correlated shadow fading," in *2012 IEEE International Conference on, Communications (ICC)*, pp. 3659 –3663, June 2012.

[17] K. Kaemarungsi and P. Krishnamurthy, "Properties of indoor received signal strength for wlan location fingerprinting," in *Mobile and Ubiquitous Systems: Networking and Services, 2004. MOBIQUITOUS 2004. The First Annual International Conference on*, pp. 14 – 23, Aug. 2004.

[18] N. Patwari and A. Hero, "Signal strength localization bounds in ad hoc and sensor networks when transmit powers are random," in *Fourth IEEE Workshop on Sensor Array and Multichannel Processing, 2006.*, pp. 299 –303, July 2006.

[19] Y. Sheng, K. Tan, G. Chen, D. Kotz, and A. Campbell, "Detecting 802.11 MAC layer spoofing using Received Signal Strength," in *The 27th Conference on Computer Communications. IEEE. INFOCOM 2008.*, pp. 1768–1776, 2008.

[20] C.-Y. Kim, D. Song, Y. Xu, and J. Yi, "Localization of multiple unknown transient radio sources using multiple paired mobile robots with limited sensing ranges," *Robotics and Automation*, 2011.

[21] J. Nelson, J. Almodovar, M. Gupta, and W. Mortensen, "Estimating multiple transmitter locations from power measurements at multiple receivers," in *IEEE International Conference on Acoustics, Speech and Signal Processing, ICASSP 2009.*, pp. 2761 –2764, April 2009.

[22] R. R. Wilcox, *Applying Contemporary Statistical Techniques*. Oxford, UK: Elsevier, 2003.

[23] R. E. Henkel, "Tests of significance," *SAGE*, vol. 4, 1976.

[24] J. T. McClave and T. Sincich, *Statistics*. Upper Saddle River, NJ: Pearson Education, 10th ed., 2006.

[25] X. Luo, W. J. OBrien, and C. L. Julien, "Comparative evaluation of received signal-strength index (rssi) based indoor localization techniques for construction jobsites," *Advanced Engineering Informatics*, 2010.

[26] J. Nelson and M. Gupta, "An EM technique for multiple transmitter localization," in *41st Annual Conference on Information Sciences and Systems, 2007. CISS '07.*, pp. 610 –615, March 2007.

[27] J. Nelson, M. Hazen, and M. Gupta, "Global optimization for multiple transmitter localization," in *Military Communications Conference, 2006. MILCOM 2006. IEEE*, pp. 1 –7, Oct. 2006.

[28] J. Nelson, M. Gupta, J. Almodovar, and W. Mortensen, "A Quasi-EM method for estimating multiple transmitter locations," *Signal Processing Letters, IEEE*, vol. 16, pp. 354 –357, May 2009.

[29] B.-C. Liu, K.-H. Lin, and J.-C. Wu, "Analysis of hyperbolic and circular positioning algorithms using Stationary Signal-Strength-Difference measurements in wireless communications," *IEEE Transactions on Vehicular Technology,*, vol. 55, pp. 499 – 509, March 2006.

[30] B.-C. Liu and K.-H. Lin, "SSSD-based mobile positioning: On the accuracy improvement issues in distance and location estimations," in *IEEE Transactions on Vehicular Technology*, vol. 58, pp. 1245–1254, March 2009.

[31] B. Liu and K. H. Lin, "Distance difference error correction by least square for stationary signal-strength-difference-based hyperbolic location in cellular communications," *IEEE Transactions on Vehicular Technology*, vol. 57, pp. 227 –238, Jan. 2008.

[32] B. Jackson, S. Wang, and R. Inkol, "Received Signal Strength Difference emitter geolocation least squares algorithm comparison," in *2011 24th Canadian Conference on Electrical and Computer Engineering (CCECE)*, pp. 001113 –001118, May 2011.

[33] S. Wang, B. R. Jackson, and R. Inkol, "Emitter geolocation estimation using power difference of arrival: An algorithm comparison for non-cooperative emitters," tech. rep., Defence Research and Development Canada, May 2011.

[34] S. Wang, R. Inkol, and B. Jackson, "Relationship between the maximum likelihood emitter location estimators based on received signal strength (RSS) and received signal strength difference (RSSD)," in *2012 26th Biennial Symposium on Communications (QBSC)*, pp. 64 –69, May 2012.

[35] S. Wang and R. Inkol, "A near-optimal least squares solution to Received Signal Strength Difference based geolocation," in *2011 IEEE International Conference on Acoustics, Speech and Signal Processing (ICASSP)*, pp. 2600 –2603, May 2011.

[36] L. Mailaender, "Geolocation Bounds for Received Signal Strength (RSS) in Correlated Shadow Fading," in *2011 IEEE Conference on Vehicular Technology(VTC Fall)*, pp. 1 –6, Sept. 2011.

[37] L. J. Bain and M. Engelhardt, *Introduction to Probability and Mathematical Statistics*. Pacific Grove, CA: Duxbury, second ed., 1992.

[38] N. Ravishanker and D. K. Dey, *A First Course in Linear Model Theory*. Boca Raton, FL: Chapman and Hall, 2002.

[39] G. H. Golub and C. F. V. Loan, *Matrix Computations*. Baltimore, MD: The Johns Hopkins Univ. Press, 1996.

[40] R. Martin, A. S. King, R. Thomas, and J. Pennington, "Practical limits in RSS-based positioning," in *IEEE International Conference on Acoustics, Speech and Signal Processing (ICASSP), 2011*, pp. 2488–2491, 2011.

[41] R. Martin, C. Anderson, R. Thomas, and A. S. King, "Modelling and analysis of radio tomography," in *2011 4th IEEE International Workshop on Computational Advances in Multi-Sensor Adaptive Processing (CAMSAP),*, pp. 377–380, 2011.

REPORT DOCUMENTATION PAGE

Form Approved
OMB No. 0704–0188

1. REPORT DATE *(DD–MM–YYYY)*	2. REPORT TYPE	3. DATES COVERED *(From — To)*
13–06–2013	Doctoral Dissertation	Sept 2009–June 2013

4. TITLE AND SUBTITLE

Development of a Model and Localization Algorithm for Received Signal Strength-Based Geolocation

5a. CONTRACT NUMBER

5b. GRANT NUMBER

5c. PROGRAM ELEMENT NUMBER

6. AUTHOR(S)

King, Amanda Sue, Civilian

5d. PROJECT NUMBER

5e. TASK NUMBER

5f. WORK UNIT NUMBER

7. PERFORMING ORGANIZATION NAME(S) AND ADDRESS(ES)

Air Force Institute of Technology
Graduate School of Engineering and Management (AFIT/EN)
2950 Hobson Way
WPAFB, OH 45433-7765

8. PERFORMING ORGANIZATION REPORT NUMBER

AFIT–ENG–DS–13–J–02

9. SPONSORING / MONITORING AGENCY NAME(S) AND ADDRESS(ES)

Intentionally left blank

10. SPONSOR/MONITOR'S ACRONYM(S)

11. SPONSOR/MONITOR'S REPORT NUMBER(S)

12. DISTRIBUTION / AVAILABILITY STATEMENT

DISTRIBUTION STATEMENT A:
APPROVED FOR PUBLIC RELEASE; DISTRIBUTION UNLIMITED

13. SUPPLEMENTARY NOTES

14. ABSTRACT

Location-Based Services (LBS), also called geolocation, have become increasingly popular in the past decades. They have several uses ranging from assisting emergency personnel, military reconnaissance and applications in social media. In geolocation a group of sensors estimate the location of transmitters using position and Radio Frequency (RF) information. A review of the literature revealed that a majority of the Received Signal Strength (RSS) techniques used made erroneous assumptions about the distribution or ignored effects of multiple transmitters, noise and multiple antennas. Further, the corresponding algorithms are often mathematically complex and computationally expensive. To address the issues this dissertation focused on RSS models which account for external factors effects and algorithms that are more efficient and accurate.

The models of RSS that were developed in this research include a multiple transmitter model, a multiple antenna model and several models using Differential Received Signal Strength (DRSS). A DRSS model produced results that were 80% more accurate when compared with a traditional path-loss RSS model for localization of multiple transmitters.

The principal contributions of this research to the community include new models for RSS and two novel algorithms used to localize RSS measurements. These contributions also included development of DRSS models and algorithms that have not previously been seen in the literature.

15. SUBJECT TERMS

geolocation, received signal strength, differential received signal strength, localization

16. SECURITY CLASSIFICATION OF:			17. LIMITATION OF ABSTRACT	18. NUMBER OF PAGES	19a. NAME OF RESPONSIBLE PERSON
a. REPORT	b. ABSTRACT	c. THIS PAGE			Dr. Richard K. Martin (ENG)
U	U	U	UU	102	19b. TELEPHONE NUMBER *(include area code)* (937) 255-3636 x4625 richard.martin@afit.edu